DIGITAL ACCESS TO SCHOLARSHIP AT HARVARD

2D-Shape Analysis Using Conformal Mapping

(Article begins on next page)

2D-Shape Analysis Using Conformal Mapping

E. SHARON AND D. MUMFORD*
Division of Applied Mathematics, Brown University, Rhode Island, Providence, 02912,

Abstract. The study of 2D shapes and their similarities is a central problem in the field of vision. It arises in particular from the task of classifying and recognizing objects from their observed silhouette. Defining natural distances between 2D shapes creates a metric space of shapes, whose mathematical structure is inherently relevant to the classification task. One intriguing metric space comes from using conformal mappings of 2D shapes into each other, via the theory of Teichmüller spaces. In this space every simple closed curve in the plane (a "shape") is represented by a 'fingerprint' which is a diffeomorphism of the unit circle to itself (a differentiable and invertible, periodic function). More precisely, every shape defines to a unique equivalence class of such diffeomorphisms up to right multiplication by a Möbius map. The fingerprint does not change if the shape is varied by translations and scaling and any such equivalence class comes from some shape. This coset space, equipped with the infinitesimal Weil-Petersson (WP) Riemannian norm is a metric space. In this space, the shortest path between each two shapes is unique, and is given by a geodesic connecting them. Their distance from each other is given by integrating the WP-norm along that geodesic. In this paper we concentrate on solving the "welding" problem of "sewing" together conformally the interior and exterior of the unit circle, glued on the unit circle by a given diffeomorphism, to obtain the unique 2D shape associated with this diffeomorphism. This will allow us to go back and forth between 2D shapes and their representing diffeomorphisms in this "space of shapes". We then present an efficient method for computing the unique shortest path, the geodesic of shape morphing between each two end-point shapes. The group of diffeomorphisms of S^1 acts as a group of isometries on the space of shapes and we show how this can be used to define shape transformations, like for instance 'adding a protruding limb' to any shape.

Keywords: group of diffeomorphisms, group of shape transformations, shape representation, metrics between shapes, conformal, Riemann mapping theorem, Weil-Petersson metric, geodesic, fingerprints of shapes

1. Introduction

Many different representations for the collection of all 2D shapes[1], and many different measures of similarity between them have been studied recently (Hildreth, 1984; Kass et al., 1988; Ullman, 1989; Amit 1991; Yuille, 1991; Sclaroff and Pentland, 1995; Kimia et al., 1995; Geiger et al., 1995; Gdalyahu and Weinshall, 1999; Basri et al., 1998; Belongie et al., 2002; Sebas-tian et al., 2001; Carlsson, 1999). Although significant progress has been made, none are fully satisfactory from the point of view of a leading to a successful classification of the collection of all shapes. In part, this shortcoming is due to the fact that human perception may give different meanings to similarity between shapes in different contexts and for different tasks (Biederman, 1985; Mumford, 1991) (see Fig. 1). In this paper, we propose the study of a new approach to measuring the similarity of shapes by applying the mathematical theory of complex analysis. This grows out of a new way of representing shapes.
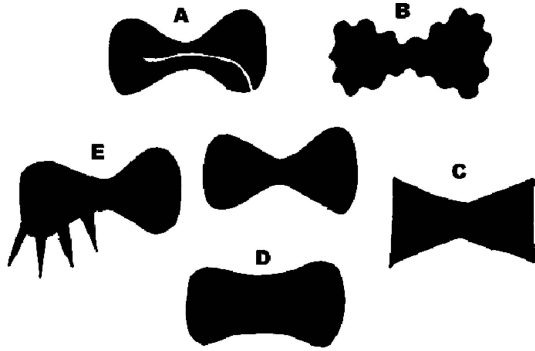
Figure 1.   All the figures **A**, **B**, **C**, **D** and **E** are similar to the middle one, but they differ in different ways. Which shapes should be considered closer may depend on context. This illustration is due to B. Kimia.

Representing shapes in a simple way for classification is difficult because of two things: on the one hand, the set of all shapes is inherently infinite dimensional and, on the other hand, it has no natural linear structure. More precisely, the first assertion means that if we map every shape to a point of $\mathbb{R}^n$ by assigning to it n features, there will always be many distinct shapes on which all these features coincide. You cannot capture all the variability of a shape in a finite set of features. The second assertion means that there is no vector space structure on the set of all shapes, no way of adding, subtracting and multiplying by scalars in this set which satisfies the vector space axioms[2]. So if we use an infinite number of features to describe shapes, such as all its moments or all its Fourier coefficients, then although we get a representation of the set of shapes in a vector space, there will be sequences of moments or Fourier coefficients which do not come from any shape. The upshot is that the set of all shapes is mathematically rather complicated. We feel this is the deep reason why shape classification algorithms in the literature have been less than perfectly satisfactory.

Although the set of shapes is nonlinear and infinite dimensional, this does not prevent it from having its own geometry. The first step towards analyzing its geometry is to endow this set with a *metric*, a numerical measure of the difference between any 2 shapes. Many metric approaches for the classification of shapes have also been suggested. The Hausdorff distance is perhaps the best known: this is a 'sup' or so called L^∞ norm. One can also take the area of the symmetric difference of the interiors of the 2 shapes: this is a L^1 type norm, gotten by a simple integral. We may also measure in some way the difference of the orientations as well as the locations of the 2 shapes: these are first derivative

norms. One can play with these alternatives and work out which shapes in Fig. 1 are closer to the central shape in which metric.

In our method of representing shapes, every shape will define a sort of 'fingerprint', which is a diffeomorphism of the unit circle to itself. Such a diffeomorphism is given by a smooth increasing function $f : \mathbb{R} \to \mathbb{R}$ which is differentiable and satisfies $f(x + 2\pi) = f(x) + 2\pi$ and two functions f_1, f_2 define the same diffeomorphism if $f_1(x) \equiv f_2(x) + 2\pi n$. The group of such diffeomorphisms will be denoted by $\mathbf{Diff}(S^1)$. The construction is based on the existence of a conformal mapping from the interior of any shape Γ to the interior of the unit disk via the Riemann mapping theorem. Like all conformal maps, it preserves the angles between any two intersecting curves and, moreover, it is unique up to composition with a Möbius-transformation ambiguity.

More precisely, we will show that every simple closed curve in the plane defines an equivalence class of diffeomorphisms *f*. These equivalence classes are the right cosets of these diffeomorphisms modulo the three dimensional subgroup of Möbius maps[3] $PSL_2(\mathbb{R})$, namely the maps from the complex unit circle $\{z \,|\, |z| = 1\}$ to itself given by $z \mapsto (az + b)/(\bar{b}z + \bar{a})$. This set of equivalence classes is then written as the *quotient* $\mathbf{Diff}(S^1)/PSL_2(\mathbb{R})$. In this assignment, two shapes Γ_1, Γ_2 define the *same* diffeomorphism only when one shape is gotten from the other by a translation and scaling, i.e. $\Gamma_2 = a \cdot \Gamma_1 + (b, c)$. If $\mathcal{S}$ is the set of 2D shapes and H is the group of maps $(x, y) \mapsto (ax + b, ay + c)$, then the result of this construction is a bijection between the two quotient sets:

$$\mathbf{Diff}(S^1)/PSL_2(\mathbb{R}) \cong \mathcal{S}/H.$$

Moreover, this quotient space turns out to be equipped with a very remarkable metric, the Weil-Petersson (WP) Riemannian metric. The resulting metric space has two major properties. First, the space has non-positive sectional curvature, and hence there exists a unique geodesic between each two shapes. Defining the integral of the WP-norm along a path as the length of this path, a geodesic is defined as the shortest path connecting the two shapes and its length is the global metric on the space of shapes. The shapes along that path represent a natural morphing of one into the other. Secondly, the resulting space is homogenous with respect to the group of diffeomorphisms operating on the cosets from the left. Thus, for example, we can transform all shapes into new

shapes by composing the coset representing them by a diffeomorphism on the left and this transformation will preserve the WP distance, take geodesics to geodesics and hence change the above morphing between any two shapes into the morphing between the transformed shapes.

It is essential in this framework to be able to move back and forth computationally between 2D shapes and the diffeomorphisms representing them. Moving from a given shape into the diffeomorphism representing it can be done by computational implementations of the Riemann mapping theorem. Several approaches to this exist in the literature, see 3.1. Perhaps the most effective way is by using a numerical implementation of the Schwarz-Christoffel formula, applied to a polygon that tightly approximates the shape (Driscoll, 1996). But going back from the diffeomorphism to the shape is a new computational challenge, known as the "welding" problem. It involves the construction of two conformal maps, one defined inside the unit circle and one outside, which differ on the unit circle by the given diffeomorphism. In this paper, we will give two approaches to computing the solution of welding problem. Having this transformation between the space of shapes and the group of diffeomorphisms, we then go on to compute geodesics in the WP-metric. We do this by computing the geodesics in the coset space $\mathbf{Diff}(S^1)/PSL_2(\mathbb{R})$ and then using welding to move this into a morphing of two plane shapes.

2. Shapes as Diffeomorphisms of the Circle

In this paper, by a "shape" we mean a simple closed smooth curve Γ in the plane. Smooth means having derivatives of all orders (i.e. being C^∞), and simple means that the curves do not intersect themselves. Everything is based on the Riemann mapping theorem which states that it is possible to map the unit disc conformally to the interior of any such shape[4]. The conformal transformation is unique up to any preceding Möbius transformations mapping the unit disc to itself (that is, maps of the form $z \mapsto (az+b)/(\bar{b}z+\bar{a})$). Conformal means that the infinitesimal angle between each two crossing curves is equal to the infinitesimal angle between the transformed curves. The nature of these mappings is shown in Fig. 2, where the image of the radial grid on the unit disc (made out of concentric circles and lines through the origin) under this map is shown. Note that the image curves remain perpendicular.
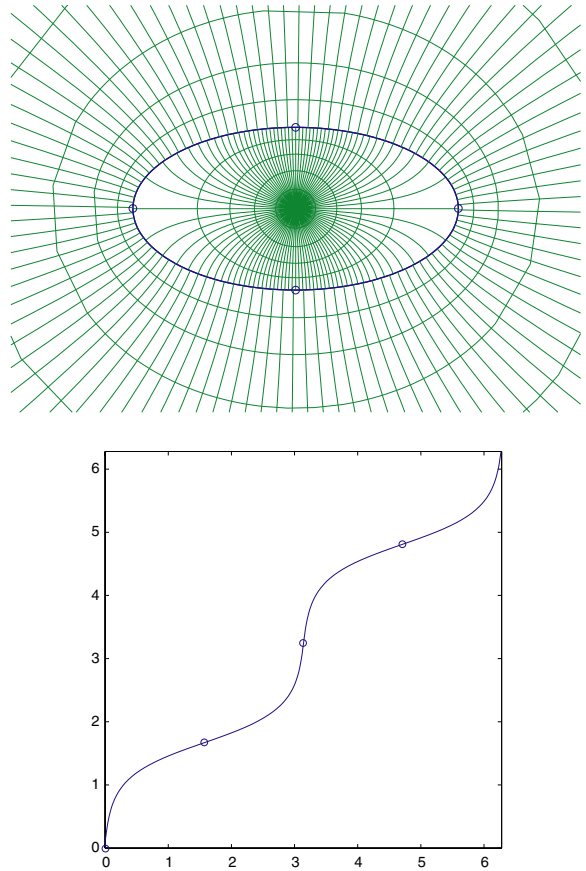

Figure 2.   On the top, the conformal parametrization of the interior and exterior of an ellipse given by the Riemann mapping theorem, shown by plotting the images under Φ_- and Φ_+ of circles around the origin and radial lines. On the bottom, the 'fingerprint' Ψ. The circled points on the 2 figures are corresponding points. Note the large derivative of the fingerprint at the points $\theta = 0, \pi$ corrsponding to the ends of the major axis and the small derivative at the points $\theta = \pi/2, 3\pi/2$ corresponding to the ends of the minor axis.

2.1. Shapes to Diffeomorphisms

In this whole paper, we associate $\mathbb{R}^2$ with the complex plane $\mathbb{C}$ and hence we denote planar points by complex numbers $u + iv$. We often want to add in the 'point at infinity'; adding this in, we get the extended complex plane, also called the Riemann sphere and denoted by $\hat{\mathbb{C}} \doteq \mathbb{C} \cup \{\infty\}$

Further, we denote the unit disc $\{z \mid |z| \leq 1\}$ by Δ_- and the infinite region outside or on the unit disc $\{z \mid |z| \geq 1\}$ (including ∞) by Δ_+. Observe that using the transformation $z \mapsto 1/z$ we can identify Δ_+ with Δ_-. For every simple closed curve Γ in $\mathbb{C}$ we denote by Γ_- its union with the region enclosed by it, and
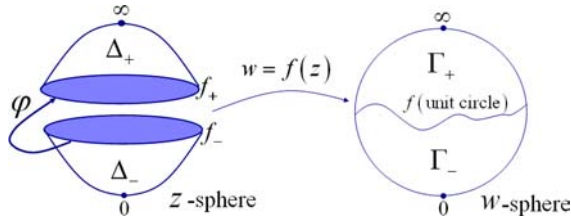
Figure 3. The conformal map *f*, as described in Sec. 2.2, maps the two halves of the *z*-sphere divided by the unit circle (left) onto the two parts of the *w*-sphere divided by Γ (right), correspondingly, such that $f_-(z) = f_+(\varphi(z))$ on $|z| = 1$.

denote by Γ_+ its union with the infinite region outside Γ (including ∞). We can think of Γ_- and Γ_+ as a partition of the Riemann sphere into two parts along Γ (see Fig. 3).

Then by the Riemann mapping theorem, for all Γ there exists a conformal map

$$\Phi_- : \Delta_- \to \Gamma_-,$$

unique up to replacing Φ_- by $\Phi_- \circ A$ for any Möbius transformations $A : \Delta_- \to \Delta_-$, $A = (az + b)/(\bar{b}z + \bar{a})$. That is, for every two conformal maps $\Phi_-^{(1)}, \Phi_-^{(2)} : \Delta_- \to \Gamma_-$ we have that $\Phi_-^{(2)-1} \circ \Phi_-^{(1)} = A$, where A is a Möbius map.

This works for Δ^+ and Γ^+ too as the point at infinity is no different from other finite points. Spelling this out, under $1/z$, Γ is transformed into the inverted simple closed curve Γ' so that Γ_+ is identified with the interior Γ'_- of Γ'. Thus we can apply the Riemann mapping theorem to get a Φ' from Δ_- and Γ'_-. Composing this conformal map with inverse on both sides, i.e. $\Phi_+(z) = 1/\Phi'(1/z)$, we get a conformal map of the exteriors

$$\Phi_+ : \Delta_+ \to \Gamma_+.$$

Φ_+ is also unique up to Möbius transformations as above. But now we can do better with Φ_+: we take the unique Möbius map A so that, replacing Φ_+ by $\Phi_+ \circ A$, we achieve the extra normalization that Φ_+ carries ∞ to ∞, and that its differential carries the real positive axis of the Δ-plane at ∞ to the real positive axis of the Γ-plane at ∞. Thus, we eliminate the Möbius ambiguity of Φ_+ for every Γ, and make Φ_+ unique. An example of this construction is shown at the top in Fig. 2, where the curve Γ is an ellipse.

The goal of this construction is to define the map

$$\Psi \doteq \Phi_+^{-1} \circ \Phi_-,$$

which it is defined on the unit circle S^1. (Note that $\Phi^-(S^1) = \Gamma$, and $\Phi_+^{-1}(\Gamma) = S^1$.) $\Psi : S^1 \to S^1$ is a diffeomorphism, which can be thought of as a periodic, real-valued function from $[0, 2\pi]$ to $[0, 2\pi]$, having a positive derivative everywhere. Ψ is a uniquely-identifying fingerprint of the shape Γ. The fingerprint of the ellipse is also shown in Fig. 2.

From the Möbius-transformation ambiguity left in Φ_- we can see that by the construction of Ψ every simple closed curve Γ induces a diffeomorphism $\Psi : S^1 \to S^1$, which is unique up to composing on the right by a diffeomorphism $\tilde{A} : S^1 \to S^1$ coming from the restriction to S^1 of any Möbius transformation $A : \Delta_- \to \Delta_-$.

If, as in the introduction, we denote the coset space[5] by $\mathbf{Diff}(S^1)/PSL_2(\mathbb{R})$ and we denote the space of simple closed smooth curves Γ by $\mathcal{S}$, then our construction of Ψ gives us the 'fingerprint' map:

$$\mathcal{S} \to \mathbf{Diff}(S^1)/PSL_2(\mathbb{R}).$$

2.2. Diffeomorphisms to Shapes: Welding

Remarkably, this map is nearly a bijection. In fact, every coset $\Psi \cdot PSL_2(\mathbb{R})$ comes from some shape Γ and two shapes Γ_1, Γ_2 give the same coset if and only if they differ by a translation and scaling. If $\overline{\mathcal{S}}$ is the quotient of shapes modulo translations and scalings, the final result is

$$\overline{\mathcal{S}} \cong \mathbf{Diff}(S^1)/PSL_2(\mathbb{R}). \tag{1}$$

To obtain Γ, Φ_- and Φ_+ corresponding to any coset, we first pick any Ψ in the coset. The 'high level' way of finding Γ is to construct an abstract Riemann surface X by 'welding' Δ_+ and Δ_- using the map Ψ to glue their boundaries together and apply the result that any Riemann surface which is topologically a 2-sphere – like X – is, in fact, conformally isomorphic to $\hat{\mathbb{C}}$ via some map Φ. Then $\Phi_\pm$ are just the restrictions of Φ to $\Delta_\pm$ and the shape Γ is nothing but the image of the unit circle in the welded surface X under Φ. This construction is illustrated in Fig. 3.

A less abstract way to prove weldings exist is to use a celebrated existence theorem of B. Bojarski and

L. Bers [9, p., 10]. We sketch the proof without details. We use the standard abreviations:

$$f_z = \frac{1}{2}(f_x - if_y), \quad f_{\bar{z}} = \frac{1}{2}(f_x + if_y).$$

The theorem states that for any $c < 1$ and any complex valued function $\mu(z)$ with $|\mu(z)| \leq c$ (called a *Beltrami differential*), the partial differential equation:

$$F_{\bar{z}} = \mu F_z,$$

has a complex valued solution[6]. We get the μ from Ψ as follows. First define $G : \Delta_- \to \Delta_-$ by:

$$G(re^{i\theta}) = re^{i\Psi(\theta)}.$$

Then let $\mu = G_{\bar{z}}/G_z$ on Δ_- (one can readily check that this works out to be $e^{i\theta}\frac{1-\Psi'}{1+\Psi'}$) and $\mu = 0$ on Δ_+. With this μ, solve the above equation for the function F. Because $\mu = 0$ on Δ_+, F must be a conformal map on Δ_+, hence it extends to ∞ and we can normalize it to have positive real derivative there. Let Φ_+ be F on Δ_+. Note that G satisfies the equation on Δ_- and, by standard arguments, any other solution there is G followed by an analytic function (that is a map with complex derivatives but which is not everywhere conformal because they can be zero). So let Φ_- be the analytic function $F \circ G^{(-1)}$ on Δ_-. Then $\Phi_- \circ G \equiv \Phi_+$ on the unit circle, as required.

2.3.   Shapes with Base Points

We have now seen that shapes, up to scaling and translation, are represented by cosets $\Psi \cdot PSL_2(\mathbb{R}) \subset \mathbf{Diff}(S^1)$. An important variant of this representation concerns shapes with base points, that is pairs $\{\Gamma, P\}$ where P is a point in the interior of Γ. The result is that shapes with base points are represented by cosets $\Psi \cdot ROT(S^1) \subset \mathbf{Diff}(S^1)$ where $ROT(S^1)$ is the group of rotations $\theta \mapsto \theta + \phi$ of the circle. Note that $ROT(S^1) \subset PSL_2(\mathbb{R})$ as the rotation through angle ϕ is given by the map $z \mapsto (az + b)/(\bar{b}z + \bar{a})$ for $a = e^{i\phi/2}, b = 0$.

This representation is a simple extension of what we have already seen: having a base point P in the interior of the shape Γ allows one to normalize the conformal map Φ_- so that $\Phi_-(0) = P$. This fixes Φ_- up to right multiplication by a rotation, hence Ψ is also determined up to such a right multiplication. This state of affairs

is often depicted by a 'commutative diagram':

$$\begin{array}{ccc} \mathbf{Diff}(S^1)/ROT(S^1) & \cong & \{\Gamma, P\}/H \\ \downarrow & & \downarrow \\ \mathbf{Diff}(S^1)/PSL_2(\mathbb{R}) & \cong & \{\Gamma\}/H \end{array}$$

where the vertical arrows denote the maps given by (i) passing from the small cosets mod *ROT* to the larger cosets mod *PSL*; and (ii) passing from a shape with base point to a shape without base point.

Closely related to this is the following remark: if a coset $\Psi \cdot PSL_2(\mathbb{R})$ represents the shape Γ, then the cosets $A \circ \Psi \cdot PSL_2(\mathbb{R})$, for various Möbius maps $A \in PSL_2(\mathbb{R})$ represent the shapes $B(\Gamma)$ for those *complex* Möbius maps $B \in PSL_2(\mathbb{C})$ such that $B_{-1}(\infty)$ lies outside Γ. Recall that complex Möbius maps are the maps of the extended complex plane given by $z \mapsto (az + b)/(cz + d)$. To see this, use the definition $\Psi = \Phi_+^{-1} \circ \Phi_-$. Then multiplying Ψ on the *right* by A is the same as replacing Φ_+ by $\Phi_+ \circ A$. Now $\Phi_+ \circ A$ is a good conformal map of the exterior of the unit circle onto the exterior of Γ, only it doesn't have the right normalization any more as it doesn't carry ∞ to ∞. In fact, $Q = \Phi_+(A(\infty))$ is some point in the exterior of Γ. Choose a complex Möbius map B so that $B^{-1}(\infty) = Q$. Further require that B^{-1} carry the positive real axis tangent direction at ∞ to the tangent direction at Q which is the image of the positive real direction under $\Phi_+ \circ A$. Then $B \circ \Phi_+ \circ A$ is fully normalized, carrying ∞ to itself and carrying the postive real direction at ∞ to itself. Thus $\Phi'_+ = B \circ \Phi_+ \circ A$ and $\Phi'_- = B \circ \Phi_-$ are the exterior and interior conformal maps for the shape $B(\Gamma)$. Thus the fingerprint of $B(\Gamma)$ is $\Psi' = (\Phi'_+)^{-1} \circ \Phi'_- = A \circ \Phi_+^{-1} \circ \Phi_- = A \circ \Psi$.

2.4.   The Homogeneous Structure of $\overline{S}$

Any group G operates, of course, on any coset space G/H by left multiplication, hence, as a result of the above construction, $\mathbf{Diff}(S^1)$ operates on the space of shapes $\overline{S}$. A concrete way of defining this action is this: to transform any $\overline{\Gamma} \in \overline{S}$ by a group element Ψ, we construct the conformal map $\Phi_+ : \Delta_+ \to \Gamma_+$ hence we get the map $\Psi' = \Phi_+ \circ \Psi \circ \Phi_+^{-1}$ from Γ to itself. Then we use the same welding trick by cutting open $\hat{\mathbb{C}}$ along Γ and rewelding it with the map Ψ'. The result can be conformally mapped to the extended sphere, taking Γ to a new curve Γ'. This way we get a *transitive* group operation on $\overline{S}$.

3.   Computing Shapes from Diffeomorphisms and Vice Versa

3.1.   *Schwarz-Christoffel: From Shapes to Diffeomorphisms*

There seem to be three published methods of computing the conformal mapping from the unit disk to the interior of a simple closed curve Γ:

1 using the Schwarz-Christoffel formula, developed by Tobin Driscoll, cf. `http://www.math.udel.edu/~driscoll/SC` and Driscoll and Trefethen (2002).
2 the method of circle packing, developed by Kenneth Stephenson, cf. `http://www.math.utk.edu/~kens/` and Stephenson (1989)
3 the 'zipper' algorithm of Donald Marshall, cf. `http://www.math.washington.edu/~marshall/zipper.html`.

The Schwarz-Christoffel method is like this: start by approximating Γ by a polygon. Let z be the complex coordinate in the unit disk, and let $\{a_i\}$ be the points on the unit circle which will map to the vertices of the polygon and let $\{\pi\alpha_i\}$ be the angles of the polygon at these vertices. Then for some C_1, C_2:

$$\Phi(z) = C_1 \int_0^z \prod_i (z - a_i)^{\alpha_i - 1} dz + C_2.$$

For instance, if the polygon is a square, then the conformal map of the unit disk to its interior is given by the elliptic integral:

$$\Phi(z) = C_1 \int_0^z \frac{dz}{\sqrt{1 - z^4}} + C_2.$$

This method has been implemented in the excellent package 'sc' by Tobin Driscoll (cited above), based on joint work with L.N. Trefethen (1996). The key problem is that one is usually given only the points $\Phi(a_i)$ and must compute $\{a_i\}$ at the same time as Φ. Moreover, they are non-unique as, for any Möbius map A, $\Phi' = \Phi \circ A$, $a_i' = A^{-1}(a_i)$ are equally good solutions. The program allows you to specify the point $\Phi(0) \in \text{Int}(\Gamma)$ to get the best looking and best behaved solution. We use this package for our examples in Section 4 below.

3.2.   *From Diffeomorphisms to Shapes: The First Method of Welding*

3.2.1. *Reducing Welding to Coupled Elliptic Boundary Value Problems.*   **Setting the equations for the conformal map f (see Fig. 3)**. We consider Δ_- and Δ_+ as a partition of the Riemann sphere into two parts along the unit circle Δ, and Γ_- and Γ_+ as a partition of the Riemann sphere into two parts along Γ, as explained in Sec. 2.1 (see Fig. 3). We associate the complex-plane variable z with the Δ-sphere, and the complex-plane variable w with the Γ-sphere. We will assume that $0 \in \Gamma_-$ in order to normalize the map Φ_- as well as Φ_+ by asking that $\Phi_-(0) = 0$. Given a diffeomorphism $\varphi : \Delta \to \Delta$, we seek a function $f(z)$ from the z-sphere minus the unit circle to the w-sphere, complex analytic on $|z| < 1$ with boundary values $f|_{|z|=1} = f_-$, and complex analytic on $|z| > 1$ with $f|_{|z|=1} = f_+$, such that

$$\begin{aligned} f(0) &= 0, \quad f(\infty) = \infty \\ f_-(z) &= f_+(\varphi(z)) \qquad |z| = 1 \end{aligned} \tag{2}$$

Defining g, a function of f which is more convenient to compute. Note that $f(z)/z$ has finite non-zero limiting values at 0 and ∞, hence it has a single-valued logarithm in Δ_- and $\Delta+$. Thus we may define $g(u)$ by

$$\log\left(\frac{f(e^u)}{e^u}\right) = g(u), u \in \widehat{\mathbb{C}} - i\mathbb{R} \tag{3}$$

so that $g(u + 2\pi i) \equiv g(u)$.

Now,

$$\begin{aligned} Re(u) \to -\infty &\quad \Rightarrow |e^u| \to 0 \\ &\Rightarrow f(e^u) \approx c_1 e^u \Rightarrow g(u) \approx \log c_1, \end{aligned} \tag{4}$$

and

$$\begin{aligned} Re(u) \to \infty &\quad \Rightarrow |e^u| \to \infty \\ &\Rightarrow f(e^u) \approx c_2 e^u \Rightarrow g(u) \approx \log c_2, \end{aligned} \tag{5}$$

for some constants c_1 and c_2. Without loss of generality, we can replace f by $c_2^{-1} f$ so that $c_2 = 1$, and $g(u) \approx 0$ as $Re(u) \to +\infty$.

We define $\Psi : \mathbb{R} \to \mathbb{R}$, satisfying $\Psi(\theta + 2\pi) = \Psi(\theta) + 2\pi$ by $\varphi(e^{i\theta}) = e^{i\Psi(\theta)}$. Then,

$$\begin{aligned} g_-(i\theta) &= \log(f_-(e^{i\theta})) - i\theta \\ &= \log(f_+(\varphi(e^{i\theta}))) - i\theta = \log(f_+(e^{i\Psi(\theta)}) - i\theta \\ &= g_+(i\Psi(\theta)) + i\Psi(\theta) - i\theta. \end{aligned} \tag{6}$$

Thus we get a new welding condition on the imaginary axis

$$g_-(i\theta) = g_+(i\Psi(\theta)) + i(\Psi(\theta) - \theta). \qquad (7)$$

Note that if Eq. 7 holds at θ then it also holds at $\theta + 2\pi$.

Setting the equations for g's imaginary part k. (h is then known from k.) Now let

$$g(u) = h(u) + ik(u), \qquad (8)$$

where h, k are real. Then,

h, k harmonic	if $Re(u) < 0, Re(u) > 0$
$h, k \to 0$	if $Re(u) \to +\infty$
$h, k \to$ suitable constants	if $Re(u) \to -\infty$ (9)
h, k periodic	if $u \to u + 2\pi i$.

Furthermore, from Eq. 7 we get that

$$\begin{aligned}
h_-(i\theta) &= h_+(i\Psi(\theta)) \\
k_-(i\theta) &= k_+(i\Psi(\theta)) + \Psi(\theta) - \theta.
\end{aligned} \qquad (10)$$

By the Cauchy-Riemann equations, if $u = s + i\theta$, we have for $s < 0, s < 0$ that

$$\frac{\partial h}{\partial \theta} = -\frac{\partial k}{\partial s}, \quad \frac{\partial h}{\partial s} = \frac{\partial k}{\partial \theta}. \qquad (11)$$

For $s = 0$ this gives

$$-\frac{\partial k_-}{\partial s} = \frac{\partial h_-}{\partial \theta} = \Psi'(\theta)\frac{\partial h_+}{\partial \theta} = -\Psi'(\theta)\frac{\partial k_+}{\partial s}. \qquad (12)$$

Thus, we can conclude the following conditions on k

k harmonic on $s < 0, \ s > 0$

k periodic w.r.t. $\theta \to \theta + 2\pi$

$k \to 0$ if $s \to \infty, k \to$ c if $s \to -\infty$ (13)

$k_-\big|_{i\theta} = k_+\big|_{i\Psi(\theta)} + \Psi(\theta) - \theta$ $\qquad$ on $s = 0$

$\frac{\partial k_-}{\partial s}\big|_{i\theta} = \Psi'(\theta)\frac{\partial k_+}{\partial s}\big|_{i\Psi(\theta)}$ $\qquad$ on $s = 0,$

for some real constant c which comes implicitly from the equations. Note that Eq. 13 is in fact an equation for a real function k, of the two real variables s and θ. Having solved it for $k = k(s, \theta)$ we get $h = h(s, \theta)$ as
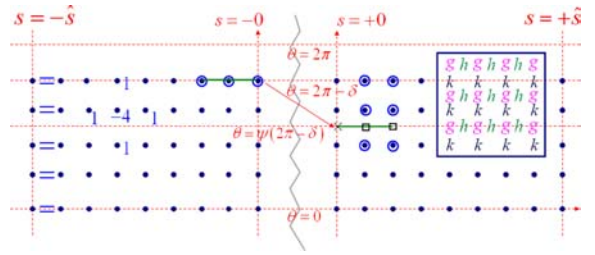

Figure 4. The (s_i, θ_j) k-grid on the (s, θ) plane. In blue over the grid points, a schematic sketch of the three types of equations involved in the numeric solution of k, as described in Sec. 3.2.2: the zero derivatives at the external boundaries ($s = \pm\hat{s}$), described by the equal signs (Neuman boundary conditions), the template of the Laplacian mask applied to internal grid points ($s \neq \pm0, \pm\hat{s}$), and the 9 grid points (circled) involved in the internal boundary condition for every internal-boundary grid point ($s = \pm 0$). The square inset demonstrates the three staggered grids, for the functions k, h and g. Every grid point is represented by the corresponding letter.

the conjugate function of k, via the Cauchy-Riemann relations in Eq. 11.

f is then known from k and h. From Eq. 3 and Eq. 8 we get that

$$f(e^{s+i\theta}) = e^{h(s+i\theta)+i(k(s+i\theta)+\theta)}. \qquad (14)$$

Since Γ is given by $f(\theta)|_{s=\pm0}$, we have that $h(\theta)|_{s=\pm0}$ and $k(\theta)|_{s=\pm0}$ describe the magnitude and angle, respectively, of the complex-plane vectors delineating Γ as a periodic function of θ.

3.2.2. Solving the Elliptic Problem Numerically

Given a diffeomorphism Ψ, we solve Eq. 13 for the θ-periodic function $k = k(s, \theta)$ on the plane branch $\theta \in [0, 2\pi]$ and $-\infty < s < \infty$. We conveniently set three different, staggered grids on (s, θ), with uniform meshsize $\delta > 0$ for the three functions k, h and g (see the square inset in Fig. 4). In practice, we cut off the s direction into $-\hat{s} \leq s \leq \hat{s}$, for some $\hat{s} > 0$, at which the values of k, h and g already converge to constants (cf. Eq. 9). Solving for k on the k-grid, we use Eq. 11 to compute h on the h-grid, and interpolating both to get g on the g-grid. It is the values of g on $s = \pm0$ that fix the resulting curve Γ. In practice, having k, we directly compute h on $s = \pm0$, at the k-grid points, as explained at the end of Sec. 3.2.2.

Solving for k: setting the s-grid and three types of numerical equations (see Fig. 4). Solving for $k(s, \theta)$, we define the (s_i, θ_j) k-grid, by indexing with $i, j \in \mathbb{N}$ an s-grid: $s_i \in \{-\hat{s}, (-\hat{s} + \delta), (-\hat{s} + 2\delta), \ldots, -2\delta, -\delta, -0, +0, \delta, 2\delta, \ldots, (\hat{s} - 2\delta), (\hat{s} - \delta), \hat{s}\}$, and a θ-grid: $\theta_j \in \{0, \delta, 2\delta, \ldots, (2\pi$

$-\delta)\}$ (for which the index j applies periodically). We set three different types of equations.

Setting the Laplacian-mask equations. First we have the basic simplest second-order discretization of the Laplace equation holding for every internal point, k being harmonic, that is: $\forall\,j$ and $\forall s_i \neq \pm\hat{s}, \pm 0$ we have

$$0 = \frac{1}{\delta^2}(-4k(s_i, \theta_j) + k(s_{i-1}, \theta_j) + k(s_{i+1}, \theta_j) \qquad (15)$$
$$+ k(s_i, \theta_{j-1}) + k(s_i, \theta_{j+1}))$$

Setting the Neuman-boundary-condition equations. Second, accounting for k's convergence to constants at $s = \pm\infty$, we set Neuman boundary conditions at the external boundaries $s_i = \pm\hat{s}$

$$k(-\hat{s}, \theta_j) = k(-\hat{s}+\delta, \theta_j) \quad \forall j$$
$$k(\hat{s}, \theta_j) = k(\hat{s}-\delta, \theta_j) \qquad \forall j \qquad (16)$$

Setting the internal-boundary-condition (welding) equations. Third, we have the k-value, and k-derivative pair of welding equations from Eq. 13, between the internal boundaries $s = -0$, associated with k_-, and $s = +0$ associated with k_+.

For every j we will associate one such pair of equations with every value $k(-0, \theta_j)$, and similarly with every value $k(+0, \theta_j)$. We separate the equations for k_- from those for k_+ because the values of $\Psi(\theta_j)$ involved in the equation for $k(-0, \theta_j)$ do not necessarily fall on some grid line $\theta_{\tilde{j}}$, since Ψ is a continuous welding diffeomorphism that does not typically send θ_j into some other grid line $\theta_{\tilde{j}}$. (Symmetrically, when focusing on the pair of welding equations for $k(+0, \theta_j)$ we may have that $\Psi^{-1}(\theta_j)$ is not a grid line.)

For every grid line θ_j we use the following second-order discretizations for $\frac{\partial k\pm}{\partial s}$

$$\frac{\partial k}{\partial s}\Big|_{(-0,\theta)} = \frac{3}{2\delta}k(-0, \theta) - \frac{2}{\delta}k(-0-\delta, \theta) \qquad (17)$$
$$+ \frac{1}{2\delta}k(-0-2\delta, \theta) + O(\delta^2),$$

and

$$\frac{\partial k}{\partial s}\Big|_{(+0,\Psi)} = -\frac{3}{2\delta}k_+|_{(+0,\Psi)} + \frac{2}{\delta}k|_{(+0+\delta,\Psi)} \qquad (18)$$
$$- \frac{1}{2\delta}k|_{(+0+2\delta,\Psi)} + O(\delta^2).$$

To replace the first term on the right, $k|_{(+0,\Psi(\theta_j))}$, we may simply use the value of k at the grid point

$(-0, \theta_j)$, via the k-value welding equation from Eq. 13

$$k_+|_{(+0,\Psi(\theta_j))} = k(-0, \theta_j) - \Psi(\theta_j) + \theta_j. \qquad (19)$$

The other two values of k participating in Eq. 18 may each be simply interpolated from the nearest three grid points along the θ-direction. We use three such values to keep an approximation of order δ^2. More precisely, for every s-column, and specifically for $s = +0 + \delta$ and $s = +0 + 2\delta$, we can write the exact interpolation relations

$$k|_{(s,\Psi)} = \frac{(\Psi - \theta_{j_2})(\Psi - \theta_{j_3})}{(\theta_{j_1} - \theta_{j_2})(\theta_{j_1} - \theta_{j_3})}k|_{(s,\theta_{j_1})} + O(\delta^2)$$
$$\frac{(\Psi - \theta_{j_1})(\Psi - \theta_{j_3})}{(\theta_{j_2} - \theta_{j_1})(\theta_{j_2} - \theta_{j_3})}k|_{(s,\theta_{j_2})} + \frac{(\Psi - \theta_{j_1})(\Psi - \theta_{j_2})}{(\theta_{j_3} - \theta_{j_1})(\theta_{j_3} - \theta_{j_2})}k|_{(s,\theta_{j_3})}, \qquad (20)$$

where $\theta_{j_1}, \theta_{j_2}$ and θ_{j_3} are the closest grid points to Ψ.

Substituting Eq. 19 and Eq. 20 in Eq. 18 we get from the last equation in Eq. 13 an equation between exactly 9 grid values. We associate this equation with the unknown $k(-0, \theta_j)$. A similar equation is associated with $k(+0, \theta_j)$ for every θ_j. Together with Eq. 15 and Eq. 16 we have thus associated one equation with every grid point (s_i, θ_j). See Fig. 4 for exemplifying the three different types of equations.

Regularizing the system of equations for k. Notice however that the solution is still not uniquely fixed. Adding a constant to any solution of this system will keep it a solution still. Thus the system is singular. So we first need to add one more equation that will determine that constant. Recalling that $k \to 0$ as $s \to \infty$ (cf. Eq. 9), a natural numerical equivalent condition would be that $\int_{\theta=0}^{2\pi} k(\infty, \theta) = 0$, and in its descretized form

$$\delta \sum_j k(\hat{s}, \theta_j) = 0. \qquad (21)$$

(We could in principle set a one grid-point value of k but this is less favorable numerically in general, and somewhat less amendable when carrying the set of differential equations in Eq. 13 to other, coarser grids.)

We now have one equation more than variables. Up to round-off errors the system has a unique solution since the equations are dependent. But for the numerical solver to work properly we add another unknown, say ϵ, to some of the equations making the new system non-singular. Since the system without this addition has a unique solution ϵ will actually turn out to be zero up to round-off errors. We have chosen to add ϵ to each

of the k-derivative welding equations, although other choices could be made as well.

Having computed k we compute h and then g, on $s = -0$. Having computed the values of k over the k-grid we note that in order to get the resulting shape Γ we only need the values of $g(s, \theta)$ and hence of $h(s, \theta)$ at either one of the internal boundaries $s = \pm 0$. We can use a discretized version of the first Cauchy-Riemann equation presented in Eq. 11 in order to approximate $\frac{\partial h}{\partial \theta}$ on $s = \pm 0$, at exactly midpoints between the k-grid points. Specifically we write

$$
\begin{aligned}
\frac{h(-0, \theta_{j+1}) - h(-0, \theta_j)}{\delta} \\
= -\frac{1}{2} \left(\frac{\partial k}{\partial s}\Big|_{(-0, \theta_{j+1})} + \frac{\partial k}{\partial s}\Big|_{(-0, \theta_j)} \right) + O(\delta^2),
\end{aligned}
\tag{22}
$$

where $\frac{\partial k}{\partial s}\Big|_{(-0, \theta_{j+1})}$ and $\frac{\partial k}{\partial s}\Big|_{(-0, \theta_j)}$ were already computed during the process of computing k, via Eq. 17. We can easily integrate the values $\{h(-0, \theta_j)\}_j$ out of their differences computed in Eq. 22, up to a global additive constant that does not matter in terms of the resulting Γ.

From $\{k(-0, \theta_j)\}_j$ and $\{h(-0, \theta_j)\}_j$ we have $\{g(-0, \theta_j)\}_j$ via Eq. 8, and can get $\{f(-0, \theta_j)\}_j$ via Eq. 3, and eventually Γ.

3.3. A Second Method of Welding

The second algorithm is based on the Hilbert transform. Recall that for functions on the real line, the Hilbert transform is convolution with the singular kernel $1/x$ and that it multiples the fourier transform of the function by $-i \cdot \text{sign}(\xi)$. In our case, we are dealing with functions on the circle and the modified Hilbert transform is convolution with $\text{ctn}(\theta/2)$ or, equivalently, multiplication of the fourier coefficients by $-i \cdot \text{sign}(n)$. For any function $f \in L^2(S^1)$, let $H(f)$ be its Hilbert transform in this sense.

Now consider the function f^+ as above. It is meromorphic on $\{|z| \geq 1\} \cup \infty$ and with a simple pole and positive real derivative at ∞, hence it has an expansion:

$$
f_+(z) = bz + a_0 + a_1 z^{-1} + a_2 z^{-2} + \cdots, \quad b > 0.
$$

Since Γ is only defined up to scalings, we can normalize so that $b = 1$. Thus, on the unit circle:

$$
f_+(e^{i\theta}) = e^{i\theta} + \sum_{n \geq 0} a_n e^{-in\theta}.
$$

Let $F(\theta) = f_+(e^{i\theta})$. Then

$$
iH(F)(\theta) = 2e^{i\theta} + a_0 - F(\theta).
$$

On the other hand, we know that f_- is holomorphic on $\{|z| \leq 1\}$, so it has the expansion:

$$
f_-(z) = c_0 + c_1 z + c_2 z^2 + \cdots.
$$

Since $f_-(e^{i\theta}) = F(\Psi(\theta))$, we get:

$$
iH(F \circ \Psi)(\theta) = (F \circ \Psi)(\theta) - c_0.
$$

Thus, by subtraction, we get:

$$
iH(F \circ \Psi) \circ \Psi^{(-1)} - iH(F) = 2F - (a_0 + c_0) - 2e^{i\theta}.
$$

We may replace F by $F - \frac{a_0 + c_0}{2}$ since Γ is only defined up to a translation. Letting $K(F) = i/2(H(F) - H(F \circ \Psi) \circ \Psi^{(-1)})$, we get the integral equation

$$
K(F) + F = e^{i\theta}
\tag{23}
$$

for F.

We can calculate K as follows. Let $\chi = \Psi_{(-1)}$ be the inverse of the welding map. Then:

$$
\begin{aligned}
K(F)(\theta_1) = {} & \frac{i}{2} \int_{S^1} \text{ctn}\left(\frac{\theta_1 - \theta_2}{2} \right) F(\theta_2) d\theta_2 \\
& - \text{ctn}\left(\frac{\chi(\theta_1) - \theta_3}{2} \right) F(\Psi(\theta_3)) d\theta_3 \\
= {} & \frac{i}{2} \int_{S^1} \left(\text{ctn}\left(\frac{\theta_1 - \theta_2}{2} \right) - \chi'(\theta_2)\text{ctn} \right. \\
& \left. \times \left(\frac{\chi(\theta_1) - \chi(\theta_2)}{2} \right) \right) F(\theta_2) d\theta_2
\end{aligned}
$$

and it is easily seen that the poles in the kernel cancel out. Remarkably, K is therefore a smooth integral operator. By the Fredholm alternative, F can be solved for as $(I + K)^{-1}(e^{i\theta})$ provided that $I + K$ has no kernel. Running the above argument backwards, it is easily seen that a function in its kernel would define a holomorphic function on the compact surface gotten by welding and this would have to be a constant. These are not in the kernel as K kills constants. Thus the welding is transformed into solving a well-posed integral equation.

Numerically, we sample F on some grid and need only convert the linear map K into a suitable matrix.

The only difficult point is to not allow the singularity of the Hilbert kernel to cause problems. To address this, we use the fact that the Hilbert kernel can be integrated explicitly:

$$\int_a^b \text{ctn}(x/2)dx = 2\log\left(\left|\frac{\sin(a/2)}{\sin(b/2)}\right|\right).$$

Note that even if $0 \in (a, b)$, the result is correct provided the intergal is taken to be its principal value (i.e. the limit of its values on the domain $[a, -\epsilon] \cup [\epsilon, b]$ as $\epsilon \to 0$.

The linear map K is then converted into a matrix as follows: let $F(\theta)$ be given at points $\theta = \theta^\alpha$, e.g. $\theta^\alpha = 2\pi\alpha/N$. Let $\theta^{\alpha+1/2} = (\theta^\alpha + \theta^{\alpha+1})/2$. The divide the interval $[0, 2\pi]$ into intervals $I_\alpha = [\theta^{\alpha-1/2}, \theta^{\alpha+1/2}]$. Assume F is approximately constant on each interval I_α. Then replacing $F(\theta_2)$ for $\theta_2 \in I_\beta$ by $F(\theta^\beta)$, and setting $\theta_1 = \theta^\alpha$, the integral for K over I_β gives the matrix entry:

$$K_{\alpha,\beta} = i \cdot \log\left|\frac{\sin(\theta^\alpha - \theta^{\beta+1/2}) \cdot \sin(\chi(\theta^\alpha) - \chi(\theta^{\beta-1/2}))}{\sin(\theta^\alpha - \theta^{\beta-1/2}) \cdot \sin(\chi(\theta^\alpha) - \chi(\theta^{\beta+1/2}))}\right|.$$

4.   Examples of Fingerprints and Their Shapes

We implemented solvers both for the welding equations described in Eq. 13, according to Sec. 3.2.2 and for Eq. 23 in Sec. 3.3. To go back and forth between $\overline{\mathcal{S}}$ and $\textbf{Diff}(S^1)/PSL_2(\mathbb{R})$ we start with a shape $\Gamma \in \overline{\mathcal{S}}$, and using the Schwarz-Christoffel transformation (Sec. 3.1) we compute the two conformal mappings, Φ_- and Φ_+ of the unit disc to the interior and exterior of the shape, correspondingly as explained in Sec. 2.1. We may then obtain a diffeomorphism Ψ from the coset in $\textbf{Diff}(S^1)/PSL_2(\mathbb{R})$ describing Γ by defining $\Psi \doteq \Phi_+^{-1} \circ \Phi_-|_{S^1}$. To go back from Ψ to Γ we follow Sec. 3.2.2 or Sec. 3.3 for welding in order to get f, and demonstrate that the resulting Γ is indeed the one we started with.

The first example is a family of shapes for which the conformal mappings Φ_- and Φ_+ can be solved analytically: these are the lens or eye shaped regions bounded by two circular arcs meeting at two corners. Figure 5 shows how the conformal map to the interior one such shape can be constructed. To get any other eye shaped region, one need only change the power in the third step and change the Möbius map used in the final step. If the angle of the eye at its corners is $\alpha\pi$, then one uses $z_3 = z_2^\alpha$. The same method gives us the
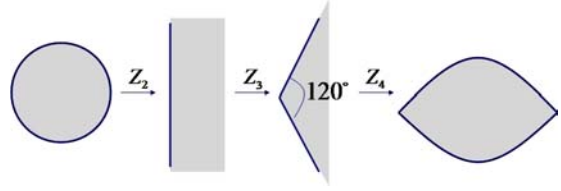

Figure 5.   Example: The construction of Φ_- – the conformal mapping of the interior of the unit disc onto the interior of the "eye" shape, presented in steps. The transformation $z_1 = e^{s+i\theta}$ carries the real-plane (s, θ) to the complex-plane circle (most left), $z_2 = \frac{1-z_1}{1+z_1}$ carries the circle to a half-plane (second left), $z_3 = z_2^{3/2}$ carries the half-plane to an "angled" half-plane (second right), and $z_4 = \frac{1-z_3}{1+z_3}$ carries the angled half-plane to the eye shape (most right). Note that the same maps take the exterior of the unit circle to the exterior of the eye, except that the middle map must be replaced by $z_3' = iz_2^{4/3}$. We can work out the fingerprint by going from z_1 to z_2 to z_3 which we equate to z_3', then back to z_2 and to z_1 without going to z_4 at all. Using the fact that if $z_1 = e^{i\theta}$, then $z_2 = -i\tan(\theta/2)$, we get the formula $\Psi(\theta) = 2\arctan(\pm|\tan(\theta/2)|^{1/2})$ where the sign is that of the tangent.

conformal to the exterior, except that as the exterior angle is $(2-\alpha)\pi$, one uses $z_3 = z_2^{2-\alpha}$. Applying this construction to both the interior and the exterior, we can verify that the fingerprints which give eye shaped regions are all of the form:

$$\Psi_\beta(\theta) = 2 \cdot \arctan\left(\tan(\theta/2)^\beta\right),$$

$$\text{where } \tan^\beta = \text{sign}(\tan)|\tan|^\beta. \qquad (24)$$

Here, if $\alpha\pi$ is the angle of the corner of the eye, then $\beta = \alpha/(2 - \alpha)$. The fingerprint for one eye shape is shown in Fig. 6.

It is striking that the formula for the fingerprint of eye-shaped regions is of the form $f^{-1}(\beta \cdot f(\theta))$: in fact define $f_1 : (0, \pi) \longleftrightarrow \mathbb{R}$ by $f_1(\theta) = \log(\tan(\theta/2))$ and $f_2 : (-\pi, 0) \longleftrightarrow \mathbb{R}$ by $f_2(\theta) = \log(-\tan(\theta/2))$. Then

$$\Psi_\beta(\theta) = \begin{cases} f_1^{-1}(\beta(f_1(\theta))) \text{ on } (0, \pi) \\ f_2^{-1}(\beta(f_2(\theta))) \text{ on } (-\pi, 0) \\ \theta \text{ if } \theta = 0 \text{ or } \pi \end{cases}$$

This formula makes apparent the identity:

$$\Psi_{\beta_1\beta_2} = \Psi_{\beta_1} \circ \Psi_{\beta_2}.$$

In this situation, the set of diffeomorphisms $\{\Psi_\beta\}$ is called a *one parameter subgroup*.

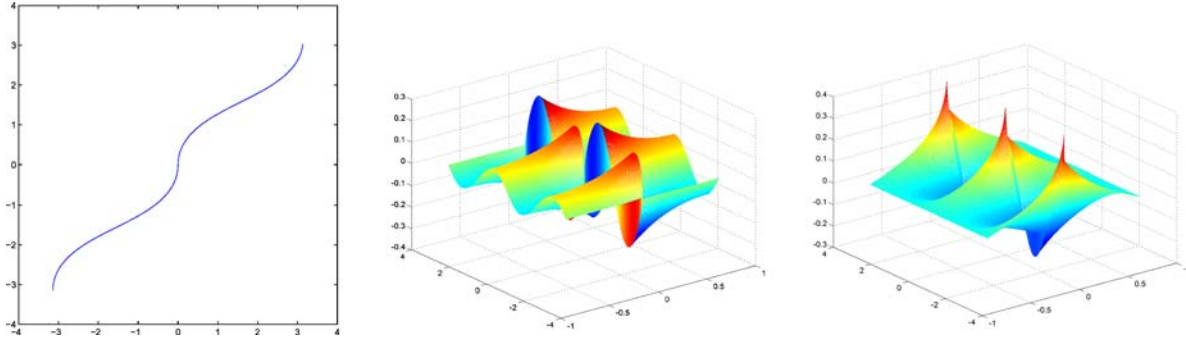All one-parameter subgroups of the group of diffeomorphisms can be gotten this way. Their additive

Figure 6.   On the left, the fingerprint of the eye shape as given by Eq. 24; in the middle and right, the functions $k(s, \theta)$ and $h(s, \theta)$ used in Sec. 3.2.2 to construct the shape from its fingerprint.

form is more general. To put the Ψ_β's in this form, it's convenient to decompose the circle into *four* intervals between the four fixed points $\{0, \pi/2, \pi, 3\pi/2\}$ of Ψ_β. Then define $g(\theta) = \log(|\log(|\tan(\theta/2)|)|)$ at all non-fixed points. Then:

$$\Psi_\beta(\theta) = \begin{cases} g^{-1}(\log(\beta) + g(\theta)), & \text{if } \theta \in ((k-1)\pi/2, k\pi/2), \text{ some } k \\ \theta \text{ if } \theta = k\pi/2, \text{ some } k. \end{cases}$$

The recipe generalizes like this: take any decomposition of the circle into a set of intervals $\{I_k = (\theta_k, \theta_{k+1})\}$. On each interval, take a bijective map $f_k : I_k \longleftrightarrow \mathbb{R}$. Then define:

$$\Psi_\alpha(\theta) = \begin{cases} f_k^{-1}(\alpha + f_k(\theta)), & \text{if } \theta \in I_k, \\ \theta, & \text{if } \theta = \theta_k, \text{ some } k. \end{cases}$$

For α infinitesimal, this diffeomorphism is given by the vector field:

$$v(\theta) = \frac{\partial}{\partial \alpha} f_k^{-1}(\alpha + f_k(\theta))\Big|_{\alpha=0} = (f_k^{-1})'(f_k(\theta)) = \frac{1}{f_k'(\theta)}.$$

In this way, every vector field v defines a one-parameter subgroup, as is well known from the theory of Lie groups.

Here's an elegant example of this: start with the Fourier basis for vector fields – $v_n(\theta) = \sin(n\theta), n \geq 2$. The zeros of these vector fields are the $2n$ points $\{\pi k/n, 0 \leq k < 2n\}$: these will be the fixed points of the corresponding one-parameter subgroups. By integrating, we solve for f_k and it comes out:

$$f_k(\theta) = \frac{1}{n} \log\left(|\tan \frac{n}{2}\theta|\right).$$

Welding, one finds wonderful n-petalled 'flowers' coming out as the corresponding shapes. As you move out on the one-parameter subgroup, increasing α, the petals start as small ripples, then extend and form alternating large circular evaginations and invaginations. This is shown in Fig. 7.

Another simple example is the square (see Fig. 8). As mentioned above, the interior and exterior conformal maps are given by simple Schwarz-Christoffel expressions[7], namely:

$$\Phi_-(z) = \int_0^z \frac{d\zeta}{\sqrt{1 - \zeta^4}}$$

$$\Phi_+(z) = z + \int_\infty^z \left(\frac{\sqrt{\zeta^4 - 1}}{\zeta^2} - 1\right) d\zeta$$

From the eye and square examples (Figs. 6 and 8), the derivative of the conformal map on the interior goes to ∞ (shown by the spreading out of the internal radial lines at the corners) while the derivative of the conformal map on the exterior goes to 0 (shown by the bunching up of the external radial lines). This is seen explicitly by noting that the derivative of the S-C formula is just its integrand and this is 0 (resp. ∞) at convex (resp. concave) corners. Thus the derivative of the fingerprint is ∞ at convex corners, 0 at concave corners. If the shape has high positive curvature at some point but not infinite as in a convex corner, we will find that the fingerprint has large derivative at the corresponding point; while points with large negative curvature, not $-\infty$ as in a concave corner, the fingerprint has very small derivative at the corresponding point.

An interesting family of fingerprints are those coming from long elongated blobs, i.e. elliptical or
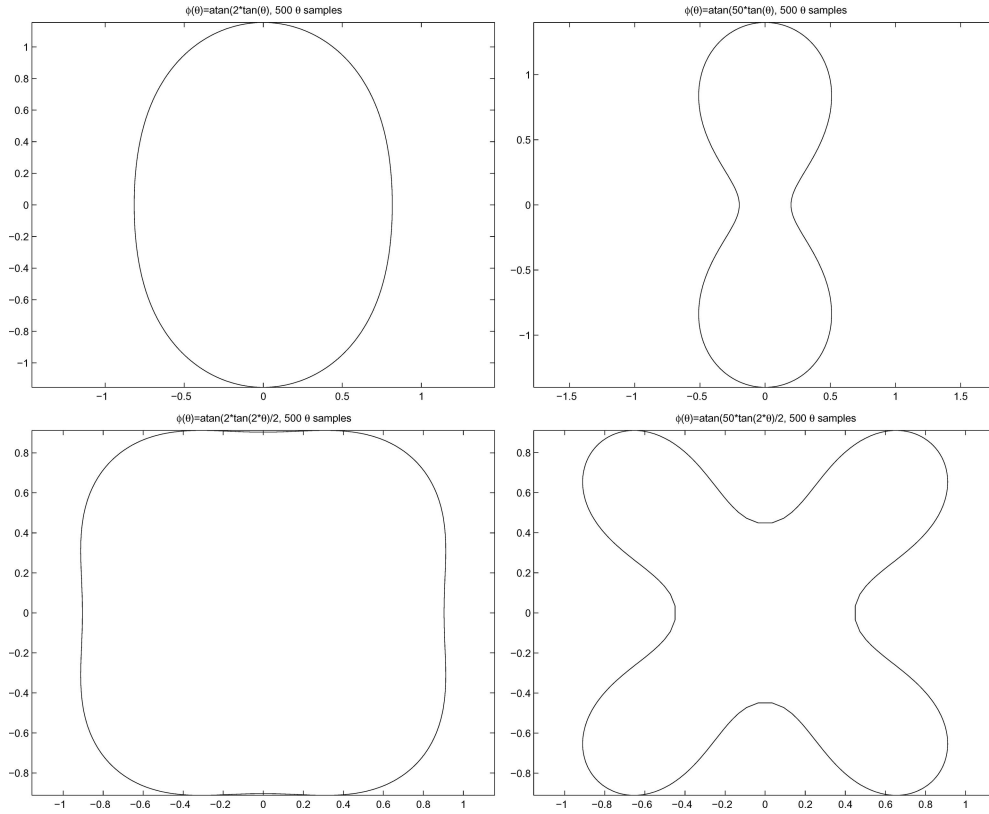
Figure 7. The shapes obtained by welding with $(2/n)\arctan(\alpha\tan(n\theta/2))$ for (n, α) equal to (2, 2) (top left), (2, 50) (top right), (4, 2) (bottom left) and (4, 50) (bottom right).

'cigar-shaped' blobs. One might have expected that these come from the one-parameter subgroup given by the vector field $\sin(2\theta)$, but, as we saw, these shapes develop concavities. This is because they are symmetrical with respect to inversion $z \mapsto 1/z$. Although the exact fingerprint for specific large eccentricity ellipses or long blobs is hard to compute exactly, the following argument gives fingerprints for one family of long blobs, as one verifies by welding. To construct this, we use 2 simple conformal maps which don't quite match up and then we force them to match up! The exterior of a circle can be mapped to the whole plane minus the slit $[-r + r]$ by the conformal map $w = (r/2)(u + 1/u)$. In this map, the exterior of a circle $|u| \geq \lambda$, for λ slightly greater than 1, is carried to the exterior of an ellipse surrounding the slit, with width $r(\lambda + 1/\lambda) \approx 2r$ and small height $r(\lambda - 1/\lambda)$. Unfortunately, the conformal map to the interior of the ellipse is not given by elementary functions. But one can map the interior of the circle to the strip $|\text{imag}(w)| < \pi$ by the map $w = 2\log((1 + z)/(1 - z))$, and this maps the interior of the circle $|z| \leq$ μ, for μ slightly less than 1, to the interior of a cigar-shaped region inside this strip. This blob has height slightly less than 2π and width $4\log((1 + \mu)/(1 - \mu))$. Both maps are illustrated in Fig. 9.

The images of these circles roughly match up if we require that $2\pi = r(\lambda - 1/\lambda)$ and $4\log(((1 + \mu)/(1-\mu)) = r(\lambda + 1/\lambda)$. We make an approximate fingerprint by mapping a point on the circle $|z| = \mu$ to that point on the circle $|u| = \lambda$ for which the *real* parts of the corresponding z-values are equal. This means:

$$\text{Re}\left(\frac{r}{2}\left(\lambda e^{i\theta_1} + \lambda^{-1}e^{-i\theta_1}\right)\right) = \text{Re}\left(2\log\left(\frac{1 + \mu e^{i\theta_2}}{1 - \mu e^{i\theta_2}}\right)\right).$$

or

$$\frac{r}{2}(\lambda + \lambda^{-1})\cos\theta_1 = \log\left(\left|\frac{1 + \mu e^{i\theta_2}}{1 - \mu e^{i\theta_2}}\right|^2\right)$$

$$= \log\left(\frac{1 + \nu\cos\theta_2}{1 - \nu\cos\theta_2}\right), \nu = \frac{2\mu}{1 + \mu^2}$$
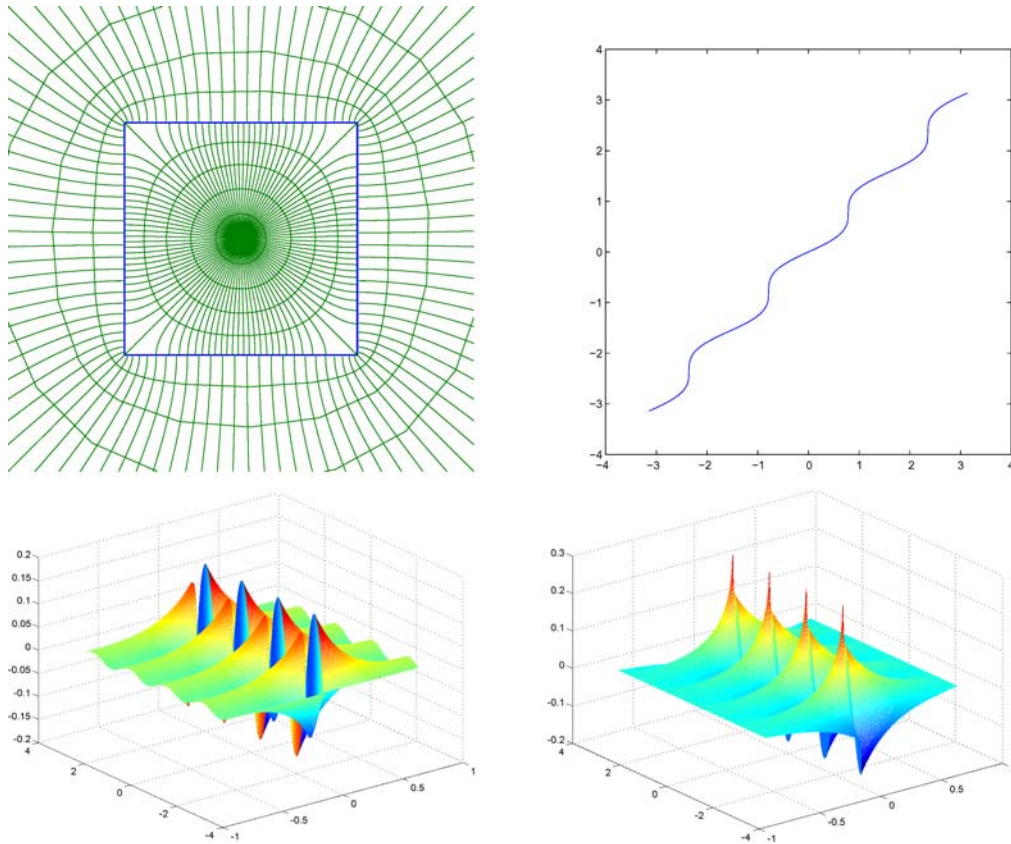
Figure 8.   On the top left, internal and external conformal parametrization of the square. Top right, the fingerprint of the square; in the bottom, the functions $k(s, \theta)$ (left) and $h(s, \theta)$ (right) used in Sec. 3.2.2 to construct the shape from its fingerprint.
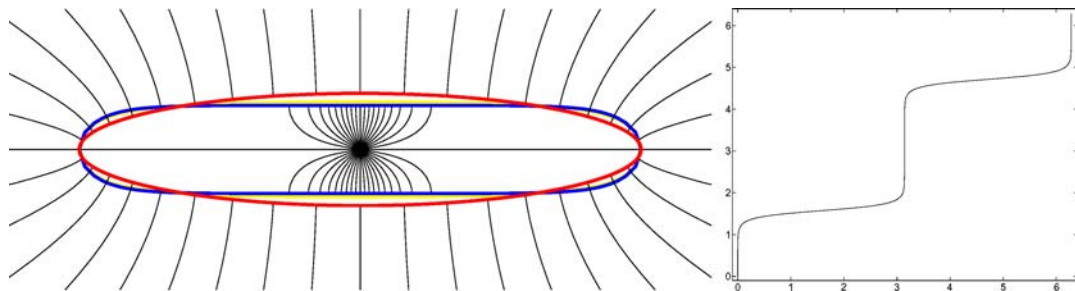

Figure 9.   The construction of an explicit formula for the fingerprint of a long blob: on the left, (i) the red curve is an ellipse and its exterior is uniformized by $w = (r/2)(u + 1/u)$, (ii) the interior of the blue curve is uniformized by the map $w = 2 \log ((1+z)/(1-z))$ applied to a circle with radius slightly less than 1. The fingerprint on the right is made by matching points on these with the same real part and the yellow curve on the left is the result of welding with this fingerprint.

Simplifying, we get the formula for the fingerprints of long blobs, Ψ_{blob1} as:

$$\theta_1 = \arccos\left(\log\left(\frac{1 + v\cos\theta_2}{1 - v\cos\theta_2}\right) \Big/ \log\left(\frac{1 + v}{1 - v}\right)\right)$$

In this form, the fingerprint has high derivatives at 2 points, corresponding to the 2 ends of the blob and the interior conformal map takes 0 to the center of the blob. The same shape, however, is defined by $\Psi_{\text{blob1}} \circ A$ for any Möbius map A. In particular, we get such a fingerprint if the interior map is chosen to take 0 to a point at

one end of the blob. Then the fingerprint will only have high derivatives at one point. With some experimentation, one finds a simple form for such a fingerprint:

$$\Psi_{\text{blob2}}(\theta) = \begin{cases} 2\arctan\left(C_1\sqrt{\log(1+a\tan^2(\theta/2))}\right), \text{ if } \theta \in [-\theta_0, \theta_0] \\ 2\arctan\left(\tan(\theta/2) + C_2\text{sign}(\theta)\right), \quad \text{ if } \theta \in (-\pi, \pi) - [-\theta_0, \theta_0] \end{cases}$$

where C_1, C_2 are chosen to make the above continuous with continuous derivatives[8].

We can use the formula for elongated blobs to illustrate the power of the group law in **Diff**(S^1). Suppose Ψ_1 and Ψ_2 are the fingerprints of 2 shapes. We can combine them in various ways using the fingerprints $\Psi_1 \circ A \circ \Psi_2$, for various Möbius maps A. As A varies, the mode of combination varies. We take $\Psi_1 = \Psi_{\text{blob2}}$ to be the fingerprint of a suitable blob and $\Psi_2 = \Psi_{\text{boom}}$ to be the fingerpint of a 'boomerang' shape computed by Schwarz-Chistoffel. To combine them, we will first pick the constants a and θ_0 in the blob fingerprint so that Ψ_{blob1} is close to the identity over much of its domain, and has very large derivative at one point. Then we combine them with a rotation R inserted. In fact, to put the boomerang back in a fixed orientation, we show in Fig. 10 the shapes defined by $R^{-1} \circ \Psi_{\text{blob1}} \circ R \circ \Psi_{\text{boom}}$. The effect will be to create a new shape in which a blob is glued to the boomerang at a point depending on where this derivative is large.

Finally, we look at two more complex shapes. The first is a silhouette of a cat. For this we apply the Schwarz-Christoffel package in order to obtain $\Psi(\theta)$. Hence $\Psi(\theta)$, $\Psi'(\theta)$ and $\Psi^{-1}(\theta)$ involved in Eq. 13 are computed numerically. We reconstrcut the shape using the first welding method. The result is shown in Fig. 11. Note again the close similarity of the computed Γ (right) to the original shape (left). Recall from Eq. 14 the way k and h (Fig. 11, bottom row) describe Γ. In our current straightforward implementation we are limited in the size of the (s, θ)-grid we can solve for. This results in the minor distortions in k, h and the resulting Γ.

The final example is the silhouette of the upper body of a person (see Fig. 12).

5.   The WP Riemannian Metric on $\overline{\mathcal{S}}$

5.1.   *The WP Norm on the Lie Algebra of Diff(S^1)*

The Lie algebra of the group **Diff**(S^1) is given by the vector space **vec**(S^1) of smooth vector fields on the circle: $v(\theta)\, \partial/\partial\, \theta$ where $v\,(\theta + 2\pi) = v(\theta)$. In general, the adjoint action of a group element $g \in G$ is the linear map from Lie(G) to itself induced by the conjugation

---

map $h \mapsto g^{-1} \circ h \circ g$ from G to itself. Explicitly, this maps $v \in \textbf{vec}(S^1)$ to $(v \circ g)/g'$, i.e. $ad_g(v) = (v \circ g)/g'$.

We can expand such a v in a Fourier series $v(\theta) = \sum_{n=-\infty}^{\infty} a_n e^{in\theta}$ (where $\overline{a_n} = a_{-n}$). The Weil-Petersson norm on $\textbf{vec}(S^1)$ is defined by:

$$||v||_{WP}^2 = \sum_{n=2}^{\infty} (n^3 - n)|a_n|^2.$$

The null space of this norm is given by those vector fields whose only Fourier coefficients are a_{-1}, a_0 and a_1, i.e. the vector fields $(a + b\cos(\theta) + c\sin(\theta))\partial/\partial\theta$, which are exactly those tangent to the Möbius subgroup $PSL_2(\mathbb{R})$, i.e. in its Lie algebra $psl_2(\mathbb{R})$.

The motivation for this particular definition is the fact that, for all $\phi \in PSL_2(\mathbb{R})$ and $v \in \textbf{vec}(S^1)$, one can verify that

$$||ad_\phi(v)||_{WP} = ||v||_{WP}.$$

5.2.   *Extending the Metric to* **Diff**(S^1)/$PSL_2(\mathbb{R})$

Riemannian metrics on coset spaces G/H which are *invariant* by all left multiplication maps $L_g : G/H \to G/H$, $g \in G$ are given by norms $||v||$ on the Lie algebra of G which are zero on the Lie subalgebra of H and which satisfy $||ad_h(v)|| = ||v||$ for all $h \in H$. Here the norm on the tangent space $T_{gH,G/H}$ to G/H at any gH is gotten from the norm on the Lie algebra via the isomorphism

$$DL_g : \text{Lie}(G)/\text{Lie}(H) = T_{eH,G/H} \to T_{gH}$$

given by the derivative of L_g at the identity e of G. In particular, this applies to **Diff**(S^1) and $PSL_2(\mathbb{R})$. Because **Diff**(S^1)/$PSL_2(\mathbb{R}) \cong \overline{\mathcal{S}}$, we have now constructed a homogeneous Riemannian metric on $\overline{\mathcal{S}}$ also.

Next let's translate this into concrete terms. Take any path $\Psi(t, \theta)$ in **Diff**(S^1), where $t \in [0, t_0] \subset \mathbb{R}$ and $\Psi(t, \theta + 2\pi) = \Psi(t, \theta) + 2\pi$. The tangent vectors to this path are given by $\frac{\partial \Psi(t,\theta)}{\partial t} = \Psi_t(t, \theta)$ or, translated back to the Lie algebra using $DL_\Psi^{(-1)}$, by
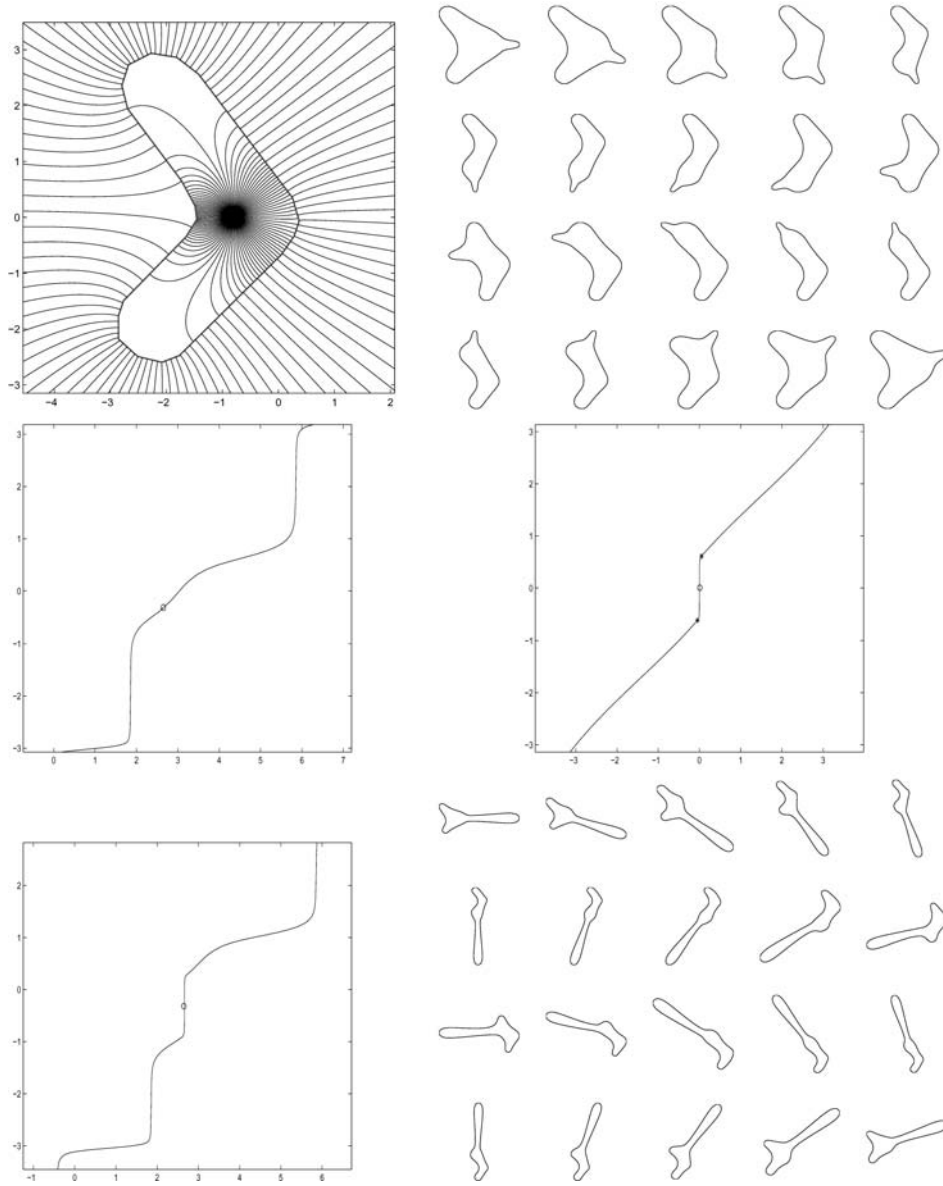
Figure 10. Top-left: the boomerang shape, middle-left: its fingerprint, middle-right: the fingerprint of the blob, and bottom-left: the fingerprint of a composition. Note the very large derivative on the boomerang fingerprint for two ends, and the very small derivative for the concave corner. The blob fingerprint has one point of high derivative corresponding to the far end, the origin being placed at the near end. A rotation is used in the composition, and the small circles mark corresponding points in the graphs of the 3 diffeomorphisms. On the top-right and bottom-right: shapes defined by compositions of the fingerprints with various rotations and constants. The composite shapes can be interpreted as the boomerang plus a blob at some point of its boundary—short on the top-right, much longer than the boomerang itself on the bottom-right. In the composite shapes on the left, the blob's constants are $a = e^{20}$, on the right $a = e^{50}$, while $\theta_0 = .05$ radians in both cases. For each set of constants, rotations through $k\,\pi/10$ radians have been put in the middle so that the protrusions are placed on the boomerang at different points of its boundary.

$\Psi_t(t, \theta)/\Psi_\theta(t, \theta)$. We expand the tangent vector at every $t \geq 0$ by its Fourier series in θ:

$$\Psi_t(t, \theta)/\Psi_\theta(t, \theta) = \sum_{n=-\infty}^{\infty} a_n(t)e^{in\theta}, \qquad (25)$$

where $a_{-n}(t) = \overline{a_n(t)}$ because the vector field is real. Its Weil-Petersson norm is then given by

$$\|\Psi_t(t, \theta)/\Psi_\theta(t, \theta)\|_{\mathrm{WP}} \doteq \sum_{n=2}^{\infty} |a_n(t)|^2(n^3 - n) \quad (26)$$
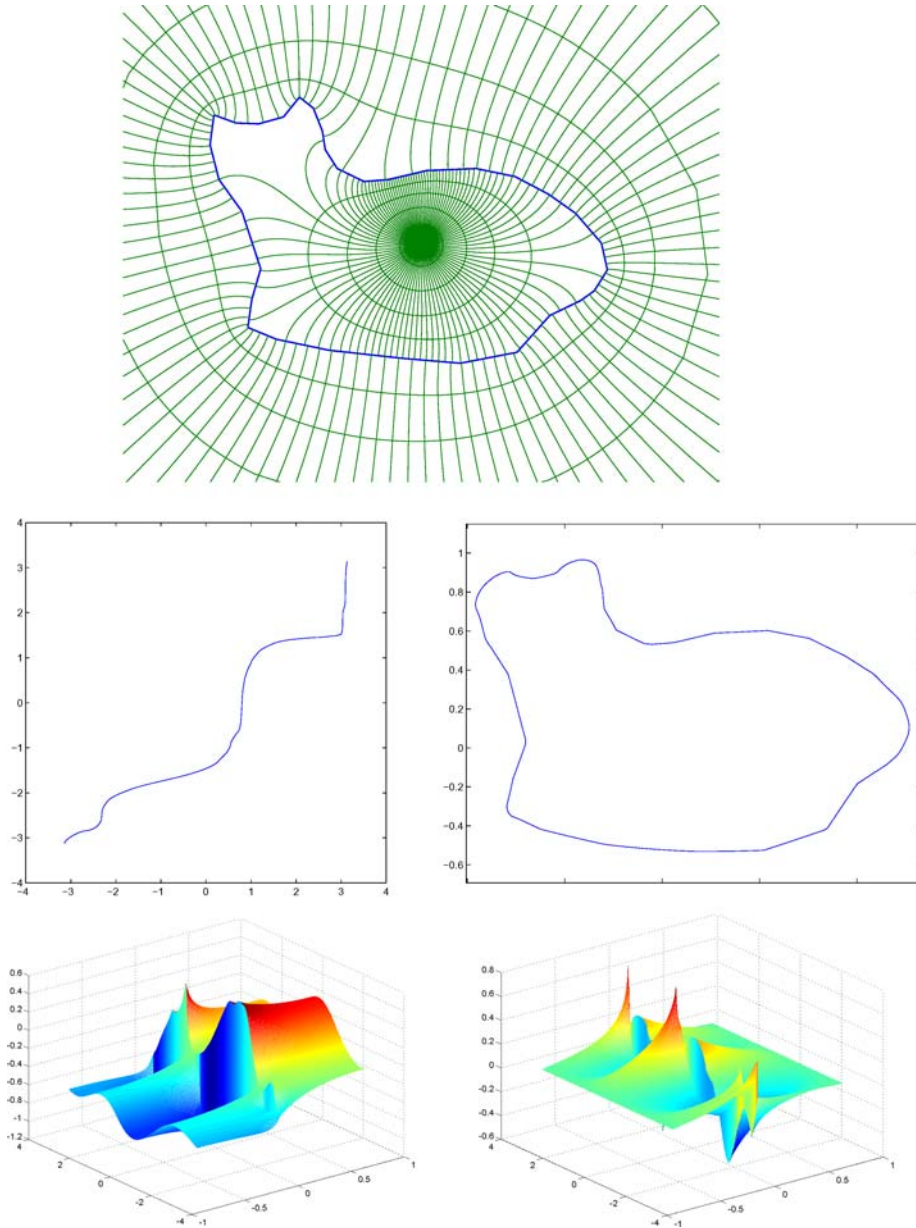
Figure 11.   Top: the conformal mappings Φ_- and Φ_+ carrying a homogenous radial grid (left, drawn schematically) onto the interior and exterior of the cat silhouette Γ; middle line: the fingerprint of the cat and the cat, as reconstructed by welding following the first method; bottom: the harmonic functions k (left) and h (right) used for reconstruction.

and the length of the path is by definition: $\int_0^{t_0} \sqrt{\sum_{n=2}^{\infty} |a_n(t)|^2 (n^3 - n)} dt$.

It is a wonderful fact that all sectional curvatures of the Weil-Petersson norm are non-positive (Bowick and Lahiri, 1988). Because of this, it is to be expected that there is a unique geodesic joining any two shapes[9] $\overline{\Gamma_1}, \overline{\Gamma_2} \in \overline{\mathcal{S}}$. Because minimizing energy and length

are equivalent, these geodesics are the solutions of the following minimization problem

$$\mathrm{Min}_{\Psi(t,\theta),t_0} \int_{t=0}^{t_0} \sum_{n=2}^{\infty} |a_n(t)|^2 (n^3 - n) dt, \qquad (27)$$

where $\Psi(0, \theta)$ and $\Psi(t_0, \theta)$ are the diffeomorphisms corresponding to the two given end-point shapes.
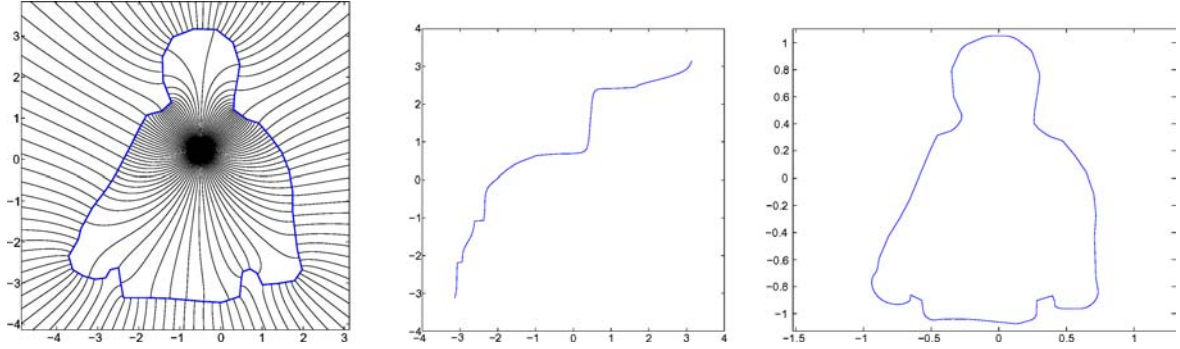
Figure 12.   A truncated human figure. On the left, the conformal parametrization of the interior and exterior; in the middle, the fingerprints; on the right, the reconstruction using the first method.

6.   Calculating the Geodesics

We solve for the geodesics $\{\Psi(t,\theta)\}_{t\in[0,1]}$, where $\Psi(t,\theta) \in \mathbf{Diff}(S^1) \; \forall \; t \in [0, 1]$, parameterized by 'time' t between the two given end-point shapes $\Psi_0 \doteq \Psi(0,\theta)$ and $\Psi_1 \doteq \Psi(1,\theta)$. The length of the geodesic between each two given end-point shapes is obtained by minimizing the Weil-Petersson norm

$$\int_0^1 \|\Psi_t(t,\theta)/\Psi_\theta(t,\theta)\|_{WP}dt, \qquad (28)$$

where Ψ_0 and Ψ_1 are the diffeomorphisms (fingerprints) corresponding to the two given end-point shapes (see Sec. 5.2).

Minimizing the norm in Eq. 28 is equivalent to minimizing the energy

$$E(\Psi_0, \Psi_1) \doteq \int_0^1 \sum_{n=2}^{\infty} |a_n(t)|^2(n^3-n)dt, \qquad (29)$$

(cf. Sec. 5.2), where

$$\Psi_t(t,\theta)/\Psi_\theta(t,\theta) = \sum_{n=-\infty}^{\infty} a_n(t)e^{in\theta} \qquad (30)$$

We discretize $t \in [0, 1]$ into M homogenously spaced points $t_u = \frac{u}{M}$, $u = 0, 1, 2, \ldots, M$, and we discretize $\theta \in [-\pi, \pi]$ into N homogenously spaced points $\theta_k = -\pi + \frac{2\pi k}{N}$, $k = 0, 2, \ldots, N-1$. We will always choose $N = 2^n$, and $M = 2^m$ for suitable n, m. We discretize the geodesics using a

(k, u)-grid into $\{\Psi(t_u, \theta_k)\}_{k,u}$, where $k = 0, 2, \ldots, N-1$, and $u = 0, 2, \ldots, M$. Both $\widetilde{\Psi}_0 \doteq \{\Psi(t_0, \theta_k)\}_k$ and $\widetilde{\Psi}_1 \doteq \{\Psi(t_M, \theta_k)\}_k$ are fixed as the end-point diffeomorphisms. In addition it is convenient for computing the energy (Eq. 29) to discretize the parameter t in the integral using also a shifted u-grid, namely an s-grid for which $t_s = \frac{1}{2M} + \frac{s}{M}$, $s = 1, 2, \ldots, M$. We denote $t_{s_-} \doteq t_s - \frac{1}{2M}$ and $t_{s_+} \doteq t_s + \frac{1}{2M}$, so that the grids s_- and s_+ coincide with points of the u grid.

We can therefore discretize

$$\Psi_\theta(t_s, \theta_k) \cong \frac{1}{2}\left(\frac{\Psi(t_{s_+}, \theta_{k+1}) - \Psi(t_{s_+}, \theta_{k-1})}{4\pi/N}\right.$$
$$\left. + \frac{\Psi(t_{s_-}, \theta_{k+1}) - \Psi(t_{s_-}, \theta_{k-1})}{4\pi/N}\right), (31)$$

and

$$\Psi_t(t_s, \theta) \cong \frac{\Psi(t_{s_+}, \theta) - \Psi(t_{s_-}, \theta)}{1/M}, \qquad (32)$$

thus obtaining the following discretization:

$$\frac{\Psi_t(t_s, \theta_k)}{\Psi_\theta(t_s, \theta_k)} \cong \left(\frac{MN}{8\pi}\right)\frac{\Psi(t_{s_+}, \theta_k) - \Psi(t_{s_-}, \theta_k)}{\Psi(t_{s_+}, \theta_{k+1}) + \Psi(t_{s_-}, \theta_{k+1}) - \Psi(t_{s_+}, \theta_{k-1}) - \Psi(t_{s_-}, \theta_{k-1})} \qquad (33)$$

To compute the geodesics $\{\Psi(t_u, \theta_k)\}_{k,u}$, we will therefore minimize the discretized version of Eq. 29

$$\widetilde{E}(\widetilde{\Psi}_0, \widetilde{\Psi}_1) \doteq \sum_{s=1}^{M}\sum_{n=2}^{N-2} |a_n(t_s)|^2(n^3-n), \qquad (34)$$
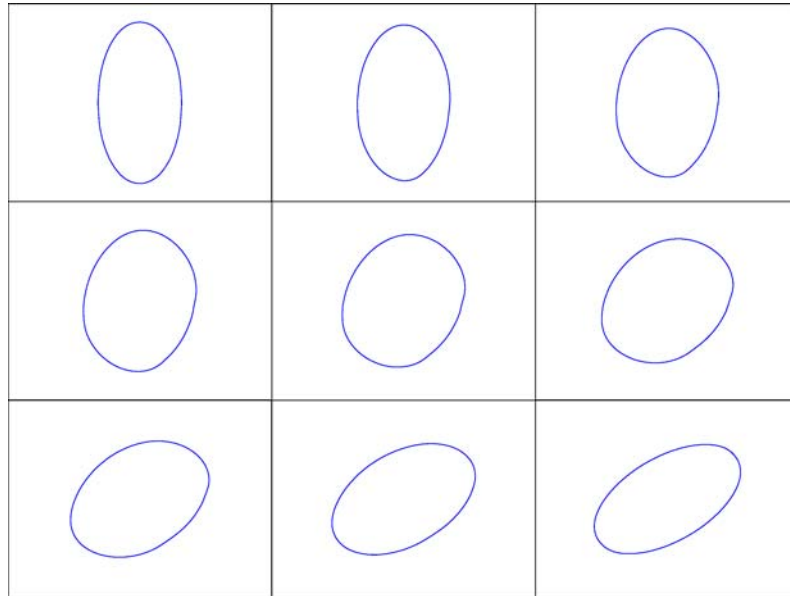
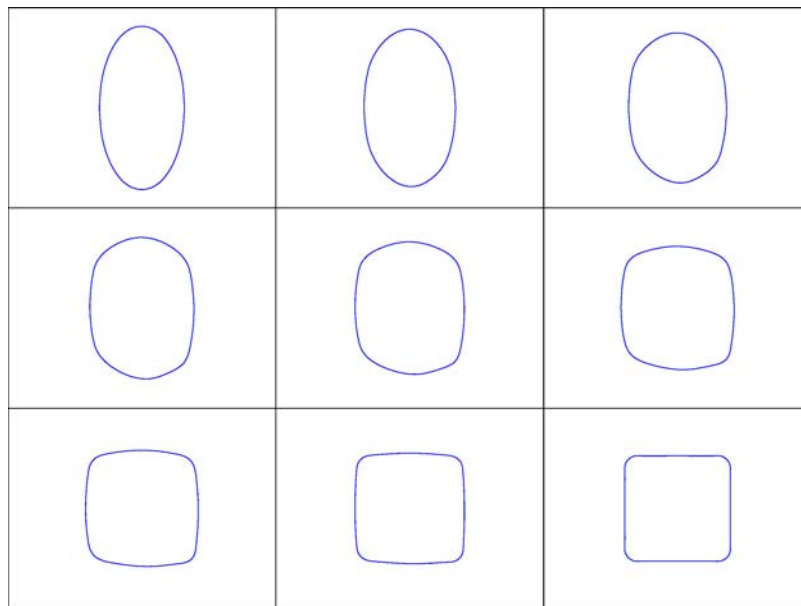*Figure 13.*   A geodesic: rotating the ellipse by $\pi/3$, clockwise.

Figure 14.   A geodesic from the ellipse with eccentricity 2 to a square.

where $\forall\, s = 1,2,\ldots, M$ and $k = 0, 1,\ldots, N-1$ we have the discrete Fourier transform

$$\frac{\Psi_t(t_s, \theta_k)}{\Psi_\theta(t_s, \theta_k)} = \frac{1}{N} \sum_{n=0}^{N/2} a_n(t_s)e^{2\pi ink/N}, \quad a_{N-n}(t_s) = \overline{a_n(t_s)}.$$

(35)

(cf. Eq. 30, but now with maximum frequency $N/2$).

We denote $\widetilde{E}_{0,1} \doteq \widetilde{E}(\widetilde{\Psi}_0, \widetilde{\Psi}_1)$, $\Psi_{k,u} \doteq \Psi(t_u, \theta_k)$, and $\Psi_{s_\pm,u} \doteq \Psi(t_{s_\pm}, \theta_k)$.

6.1.   Direct Computation of the Energy Gradient $\partial\widetilde{E}_{0,1}/\partial\Psi_{k,u}$

For introducing numerical, iterative minimization of the energy $\widetilde{E}_{0,1}$ it is useful to develop an efficient
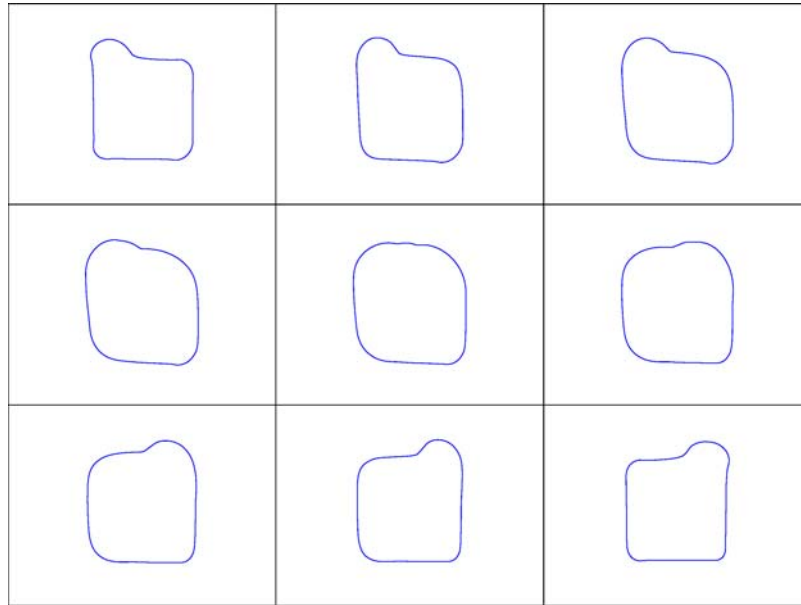
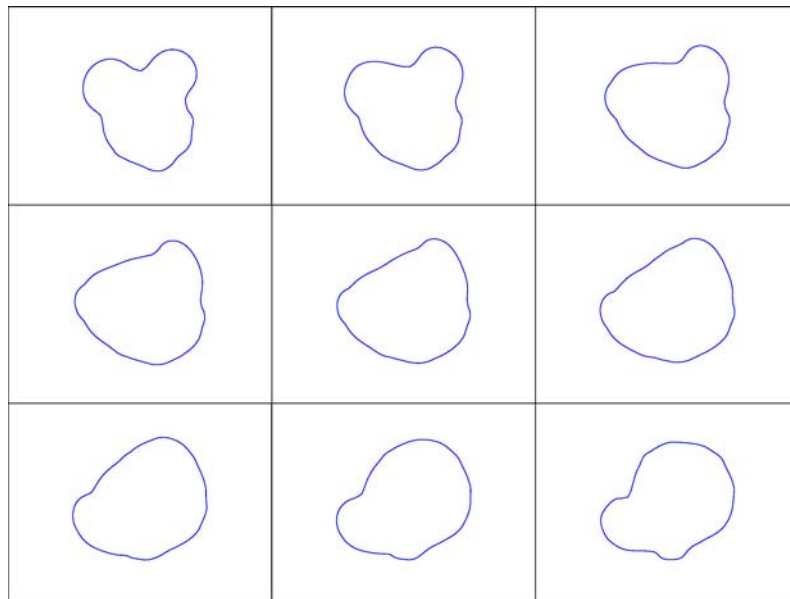*Figure 15.*   A geodesic from a square with a left bulge to the same square with a right bulge.

Figure 16.   A geodesic from a Mickey-Mouse-like shape to a Donald-Duck-like shape.

formula for directly computing its gradient $\partial \widetilde{E}_{0,1}/ \partial \Psi_{k,u}$. To obtain this we define

$$\widehat{w}_k \doteq \tilde{k}^3 - \tilde{k}, \quad \text{where } \tilde{k} = \min(k, N - k). \quad (36)$$

We then define $\{w_1\}_{1=0}^{N-1}$ to be the discrete Fourier transform of $\{\widehat{w}_l\}_{l=0}^{N-1}$. That is

$$w_l = \sum_{k=0}^{N-1} \widehat{w}_k e^{-2\pi i k l / N}. \quad (37)$$

Denoting

$$f_{k,s}(\Psi) \doteq \frac{\Psi_t(t_s, \theta_k)}{\Psi_\theta(t_s, \theta_k)}, \qquad (38)$$

we can rewrite $\widetilde{E}_{0,1}$, up to a multiplicative constant in the following way

$$\widetilde{E}_{0,1} = \sum_{i,j,s} w_{i-j} f_{i,s}(\Psi) f_{j,s}(\Psi). \qquad (39)$$

(by simply substituting Eq. 37 and Eq. 38 in Eq. 39 to satisfy Eq. 34 and Eq. 35.)

Hence

$$\frac{\partial \widetilde{E}_{0,1}}{\partial \Psi_{k,u}} = 2 \sum_{i,j,s} w_{i-j} f_{i,s}(\Psi) \frac{\partial f_{j,s}(\Psi)}{\partial \Psi_{k,u}}. \qquad (40)$$

Note that $\frac{\partial f_{j,s}(\Psi)}{\partial \Psi_{k,u}}$ for every entry (k, u) is only different from 0 in 6 of its (j, s) entries. That is, when $s_- = u$ or $s_+ = u$, and $j = k - 1, k, k + 1$. Denoting $u_\pm = u \pm \frac{1}{2M}$, we can break Eq. 40 into six sums, each of which is efficiently computed through a multiplication of a full $N \times N$ matrix of the form w_{i-j} with a sparse $N \times M$ matrix of the form $f_{i,s}$.

6.2. *Choosing a Representative Fingerprint in Each Shape Coset*

Recall that every shape is represented by an equivalence class of diffeomorphisms, namely a coset in $\mathbf{Diff}(S^1)/PSL_2(\mathbb{R})$. This creates ambiguities in the choise of fingerprint Ψ of each shape that need to be resolved before making a numerical computation of the geodesic between two shapes. The most natural way to obtain a canonical representative of each coset is to choose the unique diffeomorphism in that coset which fixes three prescribed values (angles).

Specifically, suppose the coset corresponding to a shape is given by the subset

$$\{\Psi \circ A \,|\, \Psi \in \mathbf{Diff}(S^1), A \in PSL_2(\mathbb{R})\} \subset \mathbf{Diff}(S^1).$$

For any Ψ we can find a unique A so that $\Psi \circ A$ fixes three prescribed angles, thus obtaining a unique fingerprint representation $\Psi \circ A$ for the coset $\Psi \cdot PSL_2(\mathbb{R})$.

Using Driscoll's Schwarz-Christoffel software package we compute a fingerprint Ψ for each shape, such that $\Psi(-\pi) = -\pi$. We then compose Ψ with $A \in PSL_2(\mathbb{R})$, denoting $\widehat{\Psi} \doteq \Psi \circ A$ such that

$\widehat{\Psi}(-\pi) = -\pi$, $\widehat{\Psi}(\alpha) = \alpha$ and $\widehat{\Psi}(\beta) = \beta$, where $\alpha = -\pi/4$ and $\beta = +\pi/2$. We obtain this by taking

$$A(\theta) = 2 \cdot \arctan(a + b \tan(\theta/2)), \qquad (41)$$

which satisfies $A(-\pi) = -\pi$ for every $a, b \in \mathbb{R}$, and fix a and b so that $A(\alpha) = \Psi^{-1}(\alpha)$ and $A(\beta) = \Psi^{-1}(\beta)$. That is, by Eq. 41 we solve for a and b such that

$$\begin{aligned} a + b \tan \frac{\alpha}{2} &= \tan\left(\frac{\Psi^{-1}\alpha}{2}\right) \\ a + b \tan \frac{\beta}{2} &= \tan\left(\frac{\Psi^{-1}\beta}{2}\right). \end{aligned} \qquad (42)$$

6.3. *Minimizing the Energy $\widetilde{E}_{0,1}$*

As we have seen in the previous section, we may assume that the fingerprints $\widetilde{\Psi}_0$ and $\widetilde{\Psi}_1$ of the endpoint shapes satisfy $\widetilde{\Psi}_0(-\pi) = \widetilde{\Psi}_1(-\pi) = -\pi$, $\widetilde{\Psi}_0(\alpha) = \widetilde{\Psi}_1(\alpha) = \alpha$ and $\widetilde{\Psi}_0(\beta) = \widetilde{\Psi}_1(\beta) = \beta$. We then minimize $\widetilde{E}_{0,1}$ (see Eq. 39) with all the intermediate diffeomorphisms along the geodesic keeping the three angles $-\pi$, α and β fixed. That is, we minimize $\widetilde{E}_{0,1}$ with respect to the scalar variables $\Psi(t_u, \theta_k)$, for $u = 1, 2, \ldots, M - 1$ and $k \in \{0, 1, \ldots, N - 1\}$, $k \neq 0, 3N/8, 3N/4$. For these remaining three values of k corresponding to $\theta = -\pi, \alpha, \beta$ we keep the values the diffeomorphisms fixed through the minimization, i.e. $\Psi(t_u, \theta_k) = \widetilde{\Psi}_0(t_u, \theta_k) = \widetilde{\Psi}_1(t_u, \theta_k) = -\pi, -\pi/4$ or $+\pi/2, \forall u = 1, 2, \ldots, M - 1$.

We start with $M = 8$ and $N = 64$, and set as the initial approximation for all intermediate diffeomorphisms a fingerprint of the circle shape. Specifically we set

$$\Psi(t_u, \theta_k) = \theta_k, \qquad (43)$$

for $u = 1, 2, \ldots, M - 1$ and $k = 0, 1, \ldots, N - 1$.

We then minimize $\widetilde{E}_{0,1}$ by gradient descent, starting at the current approximation to the solution (the initial approximation from Eq. 43), and minimizing the energy along the direction of the gradient (using the 'line search' method). In practice, we use the Matlab optimization function `fminnuc`. We then take this minimizing solution for $(N = 64, M = 8)$, and interpolate it in the variables $\{\theta_k\}_{k=0}^{N-1}$ to be an initial approximation for the higher resolution case, $(N = 128, M = 8)$, and minimize again the same way using `fminunc`. We interpolate into even higher resolution one more time to solve for $(N = 256, M = 8)$.

7.   Examples of Geodesics

We present 4 geodesics computed by the algorithm above (Figs. 13-16). Each of these figures should be read from left to right and top to bottom, starting at the top-left and ending at the bottom-right. Note the strong tendency to revert to shapes nearly equal to circles in the middle: this is a reflection of the fact the space of shapes is negatively curved in this metric.

8.   Summary and Conclusions

We introduce a metric space-of-shapes that arises from conformal mappings, through the mathematical theory of complex analysis. In this space, the shortest path between each two shapes is unique, and is given by a geodesic connecting them, providing a path for morphing between them. Every shape is represented in this space by an equivalence class of "fingerprints" each of which is a diffeomorphism of the unit circle to itself. We solved the welding problem to allow moving back and forth between shapes and this space-of-shapes, thus allowing the continuation of the research of shapes within this space. Indeed, our next step will be to compute the geodesics between *many different* shapes. We expect these to reflect the appealing structure-preserving properties of conformal mappings, and to be very relevant to the comparison and classification of shapes.

Notes

1. To be clear, by a shape we usually mean a smooth simple closed curve in the plane, although sometimes we mean the curve plus its interior.
2. For example, we have 'Minkowski addition' of shapes but this addition cannot have inverses because it always makes a shape bigger.
3. The reason for the notation $PSL_2(\mathbb{R})$ is that conjugating by $A = \begin{pmatrix} 1 & -i \\ 1 & i \end{pmatrix}$ takes 2×2 real matrices to the 2×2 complex matrics $\begin{pmatrix} a & b \\ \bar{b} & \bar{a} \end{pmatrix}$, so the same notation is used for both groups of matrices.
4. Smoothness of Γ is not required for Riemann's result.
5. Recall that an element in a coset space G/H is a subset $gH \doteq \{g \circ h \mid h \in H\}$ of G.
6. In fact, it is a homeomorphism and is nearly unique: if F is one solution, then $aF + b$ are all the other solutions.
7. For the modifications used in the expression for the exterior, see (Driscoll and Trefethen, 2002), p. 52.

8. In fact, if $b = a.\tan(\theta_0/2)$, $c = 1 + a.\tan^2(\theta_0/2)$, then $C_1 = \sqrt{\log c}.c/b$ and $C_2 = (\log(c/e).c + 1)/b$.
9. Because the space is infinite dimensional, this requires proof and this aspect of the metric does seem to have been discussed in the literature.

References

Amit, Y., Grenander, U., and Piccioni, M. 1991. Structural image restoration through deformable templates. *J Am Statis Assoc*, 86(414):376–387.

Basri, R., Costa, L., Geiger, D., and Jacobs, D. 1998. Determining the similarity of deformable shapes. *Vision Research*, 38:2365–2385.

Belongie, S., Malik, J., and Puzicha, J. 2002. Shape matching and object recognition using shape contexts. *PAMI*, 24(4):509–522.

Biederman, I. 1985. Human image understanding: recent research and a theory. *Computer Vision, Graphics, and Image Processing*, 32:29–73.

Bowick, M.J. and Lahiri, A. 1988. The Ricci curvature of Diff(s^1)/SL(2, R). *J. of Math. Physics*, 29:1979–1981, South Carolina.

Carlsson, S. 1999. Order structure, correspondence and shape based categories. *International Workshop on Shape, Contour and Grouping, Springer Lecture Notes in Computer Science*, p. 1681.

Driscoll. T.A. 1996. A MATLAB toolbox for Schwarz-Christoffel mapping. *ACM Trans. Math. Soft.*, 22:168–186.

Driscoll, T. and Trefethen, L.N. 2002. *Schwarz-Chrsitoffel Mapping*. Cambridge Univ. Press.

Gdalyahu, Y. and Weinshall, D. 1999. Flexible syntactic matching of curves and its application to automatichierarchical classification of silhouettes. *PAMI*, 21(12):1312–1328.

Geiger, D., Gupta, A., Costa, L., and Vlontzos, J. 1995. Dynamic programming for detecting, tracking and matching deformable contours. *IEEE Trans Pattern Anal Mach Intell*, 17(3):294–302.

Hildreth, E. 1984. *The Measurement of Visual Motion*. MIT Press, Cambridge.

Kass, M., Witkin, A., and Terzopoulos, D. 1988. Snakes: Active contour models. *IJCV*, I(4):321–331.

Kimia, B.B. Tannenbaum, A.R., and Zucker, S.W. 1995. Shapes, shocks, and deformations. *IJCV*, 15(3):189–224.

Mumford, D. 1991. Mathematical theories of shape: do they model perception? *SPIE Geom Meth Comp Vis*, 1570:2–10.

Sclaroff, S. and Pentland, A. 1995. Modal matching for correspondence and recognition. *PAMI*, 17(6):545–561.

Sebastian, T.B., Klein. P.N., and Kimia, B.B. 2001. Recognition of shapes by editing shock graphs. *ICCV*, pp. 755–762.

Stephenson, K. 2005. *Introduction to Circle Packing*. Cambridge University Press.

Ullman, S. 1989. Aligning pictorial descriptions: an approach to object recognition. *Cognition*, 32(3):193–254.

Yuille, A. 1991. Deformable templates for face recognition. *J. Cognitive Neuroscience*, 3(1):59–71.